3-1-2002

Study of the heavy flavor content of jets produced in association with W bosons in $p\bar{p}$ collisions at √s =1.8 TeV

Darin Acosta
University of Florida, acosta@phys.ufl.edu

Kenneth A. Bloom
University of Nebraska-Lincoln, kenbloom@unl.edu

Collider Detector at Fermilab Collaboration

Study of the heavy flavor content of jets produced in association with W bosons in $p\bar{p}$ collisions at $\sqrt{s} = 1.8\,\mathrm{TeV}$

D. Acosta,[12] T. Affolder,[23] H. Akimoto,[44] A. Akopian,[36] P. Amaral,[8] D. Ambrose,[31] D. Amidei,[25] K. Anikeev,[24] J. Antos,[1] G. Apollinari,[11] T. Arisawa,[44] A. Artikov,[9] T. Asakawa,[42] W. Ashmanskas,[8] F. Azfar,[29] P. Azzi-Bacchetta,[30] N. Bacchetta,[30] H. Bachacou,[23] S. Bailey,[16] P. de Barbaro,[35] A. Barbaro-Galtieri,[23] V. E. Barnes,[34] B. A. Barnett,[19] S. Baroiant,[5] M. Barone,[13] G. Bauer,[24] F. Bedeschi,[32] S. Belforte,[41] W. H. Bell,[15] G. Bellettini,[32] J. Bellinger,[45] D. Benjamin,[10] J. Bensinger,[4] A. Beretvas,[11] J. P. Berge,[11] J. Berryhill,[8] A. Bhatti,[36] M. Binkley,[11] D. Bisello,[30] M. Bishai,[11] R. E. Blair,[2] C. Blocker,[4] K. Bloom,[25] B. Blumenfeld,[19] S. R. Blusk,[35] A. Bocci,[36] A. Bodek,[35] G. Bolla,[34] Y. Bonushkin,[6] D. Bortoletto,[34] J. Boudreau,[33] A. Brandl,[27] S. van den Brink,[19] C. Bromberg,[26] M. Brozovic,[10] E. Brubaker,[23] N. Bruner,[27] E. Buckley-Geer,[11] J. Budagov,[9] H. S. Budd,[35] K. Burkett,[16] G. Busetto,[30] A. Byon-Wagner,[11] K. L. Byrum,[2] S. Cabrera,[10] P. Calafiura,[23] M. Campbell,[25] W. Carithers,[23] J. Carlson,[25] D. Carlsmith,[45] W. Caskey,[5] A. Castro,[3] D. Cauz,[41] A. Cerri,[32] J. Chapman,[25] C. Chen,[31] Y. C. Chen,[1] M. Chertok,[5] G. Chiarelli,[32] I. Chirikov-Zorin,[9] G. Chlachidze,[9] F. Chlebana,[11] L. Christofek,[18] Y. S. Chung,[35] A. G. Clark,[14] A. P. Colijn,[11] A. Connolly,[23] M. Cordelli,[13] J. Cranshaw,[39] R. Cropp,[40] D. Dagenhart,[43] S. D'Auria,[15] F. DeJongh,[11] S. Dell'Agnello,[13] M. Dell'Orso,[32] S. Demers,[36] L. Demortier,[36] M. Deninno,[3] P. F. Derwent,[11] J. R. Dittmann,[11] A. Dominguez,[23] S. Donati,[32] J. Done,[38] M. D'Onofrio,[32] T. Dorigo,[16] N. Eddy,[18] K. Einsweiler,[23] J. E. Elias,[11] E. Engels, Jr.,[33] R. Erbacher,[11] D. Errede,[18] S. Errede,[18] Q. Fan,[35] H.-C. Fang,[23] R. G. Feild,[46] J. P. Fernandez,[11] C. Ferretti,[32] R. D. Field,[12] I. Fiori,[3] B. Flaugher,[11] G. W. Foster,[11] M. Franklin,[16] J. Freeman,[11] J. Friedman,[24] Y. Fukui,[22] I. Furic,[24] S. Galeotti,[32] A. Gallas,[16,*] M. Gallinaro,[36] T. Gao,[31] A. F. Garfinkel,[34] P. Gatti,[30] C. Gay,[46] D. W. Gerdes,[25] P. Giannetti,[32] P. Giromini,[13] V. Glagolev,[9] D. Glenzinski,[11] M. Gold,[27] J. Goldstein,[11] I. Gorelov,[27] A. T. Goshaw,[10] Y. Gotra,[33] K. Goulianos,[36] C. Green,[34] G. Grim,[5] P. Gris,[11] C. Grosso-Pilcher,[8] M. Guenther,[34] G. Guillian,[25] J. Guimaraes da Costa,[16] R. M. Haas,[12] C. Haber,[23] S. R. Hahn,[11] C. Hall,[16] T. Handa,[17] R. Handler,[45] W. Hao,[39] F. Happacher,[13] K. Hara,[42] A. D. Hardman,[34] R. M. Harris,[11] F. Hartmann,[20] K. Hatakeyama,[36] J. Hauser,[6] J. Heinrich,[31] A. Heiss,[20] M. Herndon,[19] C. Hill,[5] A. Hocker,[35] K. D. Hoffman,[34] R. Hollebeek,[31] L. Holloway,[18] B. T. Huffman,[29] R. Huston,[26] J. Huth,[16] H. Ikeda,[42] J. Incandela,[11,†] G. Introzzi,[32] A. Ivanov,[35] J. Iwai,[44] Y. Iwata,[17] E. James,[25] M. Jones,[31] U. Joshi,[11] H. Kambara,[14] T. Kamon,[38] T. Kaneko,[42] K. Karr,[43] S. Kartal,[11] H. Kasha,[46] Y. Kato,[28] T. A. Keaffaber,[34] K. Kelley,[24] M. Kelly,[25] D. Khazins,[10] T. Kikuchi,[42] B. Kilminster,[35] B. J. Kim,[21] D. H. Kim,[21] H. S. Kim,[18] M. J. Kim,[21] S. B. Kim,[21] S. H. Kim,[42] Y. K. Kim,[23] M. Kirby,[10] M. Kirk,[4] L. Kirsch,[4] S. Klimenko,[12] K. Kondo,[44] J. Konigsberg,[12] A. Korn,[24] A. Korytov,[12] E. Kovacs,[2] J. Kroll,[31] M. Kruse,[10] S. E. Kuhlmann,[2] K. Kurino,[17] T. Kuwabara,[42] A. T. Laasanen,[34] N. Lai,[8] S. Lami,[36] S. Lammel,[11] J. Lancaster,[10] M. Lancaster,[23] R. Lander,[5] A. Lath,[37] G. Latino,[32] A. M. LeeIV,[10] K. Lee,[39] S. Leone,[32] M. Lindgren,[6] J. B. Liu,[35] D. O. Litvintsev,[11] O. Lobban,[39] N. Lockyer,[31] J. Loken,[29] M. Loreti,[30] D. Lucchesi,[30] P. Lukens,[11] S. Lusin,[45] L. Lyons,[29] J. Lys,[23] R. Madrak,[16] K. Maeshima,[11] P. Maksimovic,[16] L. Malferrari,[3] M. Mangano,[32] M. Mariotti,[30] G. Martignon,[30] A. Martin,[46] J. A. J. Matthews,[27] J. Mayer,[40] P. Mazzanti,[3] K. S. McFarland,[35] P. McIntyre,[38] M. Menguzzato,[30] A. Menzione,[32] P. Merkel,[11] C. Mesropian,[36] A. Meyer,[11] T. Miao,[11] R. Miller,[26] J. S. Miller,[25] H. Minato,[42] S. Miscetti,[13] M. Mishina,[22] G. Mitselmakher,[12] N. Moggi,[3] E. Moore,[27] R. Moore,[25] Y. Morita,[22] T. Moulik,[34] M. Mulhearn,[24] A. Mukherjee,[11] T. Muller,[20] A. Munar,[32] P. Murat,[11] S. Murgia,[26] J. Nachtman,[6] V. Nagaslaev,[39] S. Nahn,[46] H. Nakada,[42] I. Nakano,[17] C. Nelson,[11] D. Neuberger,[20] C. Newman-Holmes,[11] C.-Y. P. Ngan,[24] H. Niu,[4] L. Nodulman,[2] A. Nomerotski,[12] S. H. Oh,[10] Y. D. Oh,[21] T. Ohmoto,[17] T. Ohsugi,[17] R. Oishi,[42] T. Okusawa,[28] J. Olsen,[45] W. Orejudos,[23] C. Pagliarone,[32] F. Palmonari,[32] R. Paoletti,[32] V. Papadimitriou,[39] A. Parri,[13] D. Partos,[4] J. Patrick,[11] G. Pauletta,[41] C. Paus,[24] D. Pellett,[5] L. Pescara,[30] T. J. Phillips,[10] G. Piacentino,[32] K. T. Pitts,[18] A. Pompos,[34] L. Pondrom,[45] G. Pope,[33] M. Popovic,[40] F. Prokoshin,[9] J. Proudfoot,[2] F. Ptohos,[13] O. Pukhov,[9] G. Punzi,[32] A. Rakitine,[24] F. Ratnikov,[37] D. Reher,[23] A. Reichold,[29] P. Renton,[29] A. Ribon,[30] W. Riegler,[16] F. Rimondi,[3] L. Ristori,[32] M. Riveline,[40] W. J. Robertson,[10] A. Robinson,[40] T. Rodrigo,[7] S. Rolli,[43] L. Rosenson,[24] R. Roser,[11] R. Rossin,[30] C. Rott,[34] A. Roy,[34] A. Ruiz,[7] A. Safonov,[5] R. St. Denis,[15] W. K. Sakumoto,[35] D. Saltzberg,[6] A. Sansoni,[13] L. Santi,[41] H. Sato,[42] P. Savard,[40] A. Savoy-Navarro,[11] P. Schlabach,[11] E. E. Schmidt,[11] M. P. Schmidt,[46] M. Schmitt,[16,*] L. Scodellaro,[30] A. Scott,[6] A. Scribano,[32] S. Segler,[11] S. Seidel,[27] Y. Seiya,[42] F. Semeria,[3] T. Shah,[24] M. D. Shapiro,[23] P. F. Shepard,[33] T. Shibayama,[42] M. Shimojima,[42] M. Shochet,[8] A. Sidoti,[30] J. Siegrist,[23] P. Sinervo,[40] P. Singh,[18] A. J. Slaughter,[46] K. Sliwa,[43] C. Smith,[19] F. D. Snider,[11] A. Solodsky,[36] J. Spalding,[11] T. Speer,[14] P. Sphicas,[24] F. Spinella,[32] M. Spiropulu,[8] L. Spiegel,[11] J. Steele,[45] A. Stefanini,[32] J. Strologas,[18] F. Strumia,[14] K. Sumorok,[24] T. Suzuki,[42] T. Takano,[28] R. Takashima,[17] K. Takikawa,[42] P. Tamburello,[10] M. Tanaka,[42] B. Tannenbaum,[6] M. Tecchio,[25] R. J. Tesarek,[11] K. Terashi,[36] S. Tether,[24] A. S. Thompson,[15] R. Thurman-Keup,[2] P. Tipton,[35] S. Tkaczyk,[11] D. Toback,[38] K. Tollefson,[35] A. Tollestrup,[11] D. Tonelli,[32] W. Trischuk,[40] J. F. de Troconiz,[16] J. Tseng,[24] D. Tsybychev,[11] N. Turini,[32] F. Ukegawa,[42] T. Vaiciulis,[35] J. Valls,[37] G. Velev,[11] G. Veramendi,[23] I. Vila,[7] R. Vilar,[7] M. von der Mey,[6] D. Vucinic,[24] R. G. Wagner,[2] R. L. Wagner,[11] N. B. Wallace,[37] Z. Wan,[37] C. Wang,[10] M. J. Wang,[1] S. M. Wang,[12] B. Ward,[15] S. Waschke,[15] T. Watanabe,[42] D. Waters,[29] T. Watts,[37] R. Webb,[38] H. Wenzel,[20] A. B. Wicklund,[2] E. Wicklund,[11] T. Wilkes,[5] H. H. Williams,[31] P. Wilson,[11] D. Winn,[25] S. Wolbers,[11] D. Wolinski,[25] J. Wolinski,[26] S. Wolinski,[25] S. Worm,[37] X. Wu,[14] J. Wyss,[32] W. Yao,[23] P. Yeh,[1] J. Yoh,[11] C. Yosef,[26] T. Yoshida,[28] I. Yu,[21] S. Yu,[31] Z. Yu,[46] A. Zanetti,[41] F. Zetti,[23] and S. Zucchelli[3]

65 052007-1

(CDF Collaboration)

[1]*Institute of Physics, Academia Sinica, Taipei, Taiwan 11529, Republic of China*

[2]*Argonne National Laboratory, Argonne, Illinois 60439*

[3]*Istituto Nazionale di Fisica Nucleare, University of Bologna, I-40127 Bologna, Italy*

[4]*Brandeis University, Waltham, Massachusetts 02254*

[5]*University of California at Davis, Davis, California 95616*

[6]*University of California at Los Angeles, Los Angeles, California 90024*

[7]*Instituto de Fisica de Cantabria, CSIC–University of Cantabria, 39005 Santander, Spain*

[8]*Enrico Fermi Institute, University of Chicago, Chicago, Illinois 60637*

[9]*Joint Institute for Nuclear Research, RU-141980 Dubna, Russia*

[10]*Duke University, Durham, North Carolina 27708*

[11]*Fermi National Accelerator Laboratory, Batavia, Illinois 60510*

[12]*University of Florida, Gainesville, Florida 32611*

[13]*Laboratori Nazionali di Frascati, Istituto Nazionale di Fisica Nucleare, I-00044 Frascati, Italy*

[14]*University of Geneva, CH-1211 Geneva 4, Switzerland*

[15]*Glasgow University, Glasgow G12 8QQ, United Kingdom*

[16]*Harvard University, Cambridge, Massachusetts 02138*

[17]*Hiroshima University, Higashi-Hiroshima 724, Japan*

[18]*University of Illinois, Urbana, Illinois 61801*

[19]*The Johns Hopkins University, Baltimore, Maryland 21218*

[20]*Institut für Experimentelle Kernphysik, Universität Karlsruhe, 76128 Karlsruhe, Germany*

[21]*Center for High Energy Physics, Kyungpook National University, Taegu 702-701, Korea,*
Seoul National University, Seoul 151-742, Korea,
and SungKyunKwan University, Suwon 440-746, Korea

[22]*High Energy Accelerator Research Organization (KEK), Tsukuba, Ibaraki 305, Japan*

[23]*Ernest Orlando Lawrence Berkeley National Laboratory, Berkeley, California 94720*

[24]*Massachusetts Institute of Technology, Cambridge, Massachusetts 02139*

[25]*University of Michigan, Ann Arbor, Michigan 48109*

[26]*Michigan State University, East Lansing, Michigan 48824*

[27]*University of New Mexico, Albuquerque, New Mexico 87131*

[28]*Osaka City University, Osaka 588, Japan*

[29]*University of Oxford, Oxford OX1 3RH, United Kingdom*

[30]*Universita di Padova, Istituto Nazionale di Fisica Nucleare, Sezione di Padova, I-35131 Padova, Italy*

[31]*University of Pennsylvania, Philadelphia, Pennsylvania 19104*

[32]*Istituto Nazionale di Fisica Nucleare, University and Scuola Normale Superiore of Pisa, I-56100 Pisa, Italy*

[33]*University of Pittsburgh, Pittsburgh, Pennsylvania 15260*

[34]*Purdue University, West Lafayette, Indiana 47907*

[35]*University of Rochester, Rochester, New York 14627*

[36]*Rockefeller University, New York, New York 10021*

[37]*Rutgers University, Piscataway, New Jersey 08855*

[38]*Texas A&M University, College Station, Texas 77843*

[39]*Texas Tech University, Lubbock, Texas 79409*

[40]*Institute of Particle Physics, University of Toronto, Toronto M5S 1A7, Canada*

[41]*Istituto Nazionale di Fisica Nucleare, University of Trieste/Udine, Italy*

[42]*University of Tsukuba, Tsukuba, Ibaraki 305, Japan*

[43]*Tufts University, Medford, Massachusetts 02155*

[44]*Waseda University, Tokyo 169, Japan*

[45]*University of Wisconsin, Madison, Wisconsin 53706*

[46]*Yale University, New Haven, Connecticut 06520*

We present a detailed examination of the heavy flavor content of the W+jet data sample collected with the Collider Detector at Fermilab during the 1992–1995 collider run at the Fermilab Tevatron. Jets containing heavy flavor quarks are selected via the identification of secondary vertices or semileptonic decays of b and c quarks. There is generally good agreement between the rates of secondary vertices and soft leptons in the data and in the standard model simulation including single and pair production of top quarks. An exception is the number of events in which a single jet has both a soft lepton and a secondary vertex tag. In W+2,3 jet data, we find 13 such events where we expected 4.4 ± 0.6 events. The kinematic properties of this small sample of events are statistically difficult to reconcile with the simulation of standard model processes.

I. INTRODUCTION

The production of W bosons in association with jets in $p\bar{p}$ collisions at the Fermilab Tevatron Collider provides the opportunity to test many standard model (SM) [1] predictions. Previous Collider Detector at Fermilab (CDF) measurements [2] of the inclusive W cross section and of the yield of W+jet events as a function of the jet multiplicity and transverse momentum show agreement between data and the electroweak and QCD predictions of the standard model. In this study we extend the analysis of the jets associated with W boson production to include the properties of heavy flavor jets identified by the displaced vertex or the semileptonic decay of charmed and beauty quarks.

The present data set consists of 11 076 $W \to l\nu$ ($l = e$ or μ) candidates produced in association with one or more jets selected from $105 \pm 4.0 \, \text{pb}^{-1}$ of data collected by the CDF experiment at the Fermilab Tevatron [3]. The b- and c-quark content of this data set has been evaluated several times as we improved our understanding of systematic effects [4–7]. We use two different methods for identifying (tagging) jets produced by these heavy quarks. The first method uses the CDF silicon microvertex detector (SVX) to locate secondary vertices produced by the decay of b and c hadrons in a jet. These vertices (SECVTX tags) are separated from the primary event vertex as a result of the long b- and c-hadron lifetimes. The second technique is to search a jet for leptons (e or μ) produced by the semileptonic decay of b and c hadrons. We refer to these as "soft lepton tags" (SLT's) because these leptons typically have low momentum compared to leptons from W decays. Heavy flavors in W+jet events are mainly contributed by the production and decay of top quarks, by direct Wc production, and by the production of Wg states in which the gluon branches into a heavy-quark pair (gluon splitting).

A recent comparison between measured and predicted rates of W+jet events with heavy flavor as a function of the jet multiplicity is presented in Ref. [7]. The focus of that paper, as well as previous CDF publications [4–6], is the measurement of the $t\bar{t}$ production cross section. By attributing all the excess of $W + \geq 3$ jet events with a SECVTX tag over the SM background to $t\bar{t}$ production, we find $\sigma_{t\bar{t}}^- = 5.08 \pm 1.54 \, \text{pb}$ in good agreement with the average theoretical prediction, which is 5.1 pb with a 15% uncertainty [8]. We derive a numerically larger but not inconsistent value of the cross section, $\sigma_{t\bar{t}}^- = 9.18 \pm 4.26 \, \text{pb}$, when using events with one or more SLT tags. The DØ Collaboration has also measured the $t\bar{t}$ production cross section using various techniques [9]. DØ has no measurement based upon displaced secondary vertices, but using $W + \geq 3$ jet events with a muon

tag finds $\sigma_{t\bar{t}}^- = 8.2 \pm 3.5 \, \text{pb}$. In the present study, we adopt a different approach to the study of the W+jet sample and use the theoretical estimate of $\sigma_{t\bar{t}}^-$ to test if the SM prediction is compatible with the observed yield of different tags as a function of the jet multiplicity. This is of interest for top quark studies and searches for new physics, since some mechanisms proposed to explain the electroweak symmetry breaking, such as the Higgs mechanism [10] or the dynamics of a new interaction [11], predict the existence of new particles which can be produced in association with a W boson and decay into $b\bar{b}$.

Following a description of the CDF detector in Sec. II, Sec. III describes the triggers and the reconstruction of leptons, jets, and the missing transverse energy. The selection of the W+jet sample is described in Sec. IV, which also contains a discussion of the algorithms used for the heavy flavor identification followed by a description of the Monte Carlo generators and the detector simulation used to model these events. In Sec. V we summarize the method used in Ref. [7] to predict the number of W+jet events with heavy flavor and then compare the observed yield of different tags as a function of the jet multiplicity to the SM prediction, including single and pair production of top quarks. Following this comparison, in Sec. VI we study the yield of W+jet events with a SECVTX and a SLT tag in the same jet (supertag[1]); jets with a supertag will be referred to as superjets in the following. Since the semileptonic branching ratios of b and c hadrons are very well measured [12], the measurement of the fraction of jets tagged by SECVTX which contain a soft lepton tag provides an additional test of our understanding of the heavy flavor composition of this data sample. The number of these events in the $W + 2$ and $W + 3$ jet topologies is larger than the SM prediction. In Sec. VII we compare kinematic distributions of the events with a superjet to the simulation prediction. As a check, we also compare the simulation to a complementary sample of data. We find that the SM simulation models well the kinematics of the complementary sample, but does not describe properly the characteristics of the events with a superjet. Some properties of the primary and soft leptons are discussed in Sec. VIII, while Sec. IX contains a study of other properties of the superjets. In Sec. X we investigate the dependence of this study on the criteria used to select the data. Section XI summarizes our conclusions.

II. THE CDF DETECTOR

CDF is a general purpose detector designed to study $p\bar{p}$ interactions. A complete description of the CDF detector can be found in Refs. [4,13]. The detector components most relevant to this analysis are summarized below. The CDF de-

---

*Present address: Northwestern University, Evanston, Illinois 60208.

†Present address: University of California, Santa Barbara, CA 93106.

---

[1]The prefix "super" is used as a generalized term of high quality for historical reasons and is not meant as a reference to supersymmetry.

tector has azimuthal and forward-backward symmetry. A superconducting solenoid of length 4.8 m and radius 1.5 m generates a 1.4 T magnetic field. Inside the solenoid there are three types of tracking chambers for detecting charged particles and measuring their momenta. A four-layer silicon microstrip vertex detector surrounds the beryllium beam pipe of radius 1.9 cm. The SVX has an active length of 51 cm; the four layers of the SVX are at distances of 2.9, 4.2, 5.5, and 7.9 cm from the beamline. Axial microstrips with 60 μm pitch provide accurate track reconstruction in the plane transverse to the beam [14]. Outside the SVX there is a vertex drift chamber (VTX) which provides track information up to a radius of 22 cm and for pseudorapidity $|\eta| \leq 3.5$. The VTX measures the z position (along the beamline) of the primary vertex. Both the SVX and VTX are mounted inside the CTC, a 3.2-m-long drift chamber with an outer radius of 132 cm, containing 84 concentric, cylindrical layers of sense wires, which are grouped into alternating axial and stereo superlayers. The solenoid is surrounded by sampling calorimeters used to measure the electromagnetic and hadronic energy of jets and electrons. The calorimeters cover the pseudorapidity range $|\eta| \leq 4.2$. The calorimeters are segmented into η-ϕ towers that point to the nominal interaction point. There are three separate η regions of calorimeters. Each region has an electromagnetic calorimeter [central (CEM), plug (PEM), and forward (FEM)] and behind it a hadron calorimeter [central (CHA), plug (PHA), and forward (FHA), respectively]. Located six radiation lengths inside the CEM calorimeter, proportional wire chambers (CES) provide shower-position measurements in the z and $r - \phi$ view. Proportional chambers (CPR) located between the solenoid and the CEM detect early development of electromagnetic showers in the solenoid coil. These chambers provide $r - \phi$ information only.

The calorimeters act as a first hadron absorber for the central muon detection system which covers the pseudorapidity range $|\eta| \leq 1.0$. The calorimeters act as a first hadron absorber for the muon detectors which surround them. The central muon system (CMU), consisting of four layers of drift chambers covering $|\eta| \leq 0.6$, can be reached by muons with $p_T \geq 1.4$ GeV/c. The CMU detector is followed by 0.6 m of steel and four additional layers of drift chambers (CMP). The central muon extension (CMX) covers approximately 71% of the solid angle for $0.6 \leq |\eta| \leq 1.0$ with a system of drift chambers sandwiched between scintillators.

III. DATA COLLECTION AND IDENTIFICATION OF JETS AND LEPTONS

The selection of W+jet events is based upon the identification of electrons, muons, missing energy, and jets. Below we discuss the criteria used to select these objects.

A. Triggers

The data acquisition is triggered by a three-level system designed to select events that can contain electrons, muons, jets, and missing transverse energy ($\not{E}_T$). Central electrons are defined as CEM clusters with $E_T \geq 18$ GeV and a reconstructed track with $p_T \geq 13$ GeV/c pointing to it. The ratio of

hadronic to electromagnetic energy in the cluster (E_{had}/E_{em}) is required to be less than 0.125. Plug electrons, used for checks, have a higher transverse energy threshold ($E_T \geq 20$ GeV). The inclusive muon trigger requires a match of better than 10 cm in $r\Delta\phi$ between a reconstructed track with $p_T \geq 18$ GeV/c, extrapolated to the radius of the muon detector, and a track segment in the muon chambers. Calorimeter towers are combined into electromagnetic and jetlike clusters by the trigger system, which also provides an estimate of $\not{E}_T$. Trigger efficiencies have been measured using the data and are included in the detector simulation.

B. Electron selection

We use electrons in the central pseudorapidity region ($|\eta| \leq 1.0$). Stricter selection cuts are applied to central electrons which passed the trigger prerequisites. The following variables are used to discriminate against charged hadrons: (1) the ratio of hadronic to electromagnetic energy of the cluster, E_{had}/E_{em}; (2) the ratio of cluster energy to track momentum, E/P; (3) a comparison of the lateral shower profile in the calorimeter cluster with that of test-beam electrons, L_{shr}; (4) the distance between the extrapolated track position and the CES measurement in the $r - \phi$ and z views, Δx and Δz, respectively; (5) a χ^2 comparison of the CES shower profile with that of test-beam electrons, χ^2_{strip}; (6) the distance between the interaction vertex and the reconstructed track in the z-direction, z-vertex match; and (7) the isolation I defined as the ratio of additional transverse energy in a cone of radius $R = \sqrt{(\Delta\phi)^2 + (\Delta\eta)^2} = 0.4$ around the electron direction to the electron transverse energy. Fiducial cuts on the shower position measured by the CES are applied to ensure that the electron candidate is away from calorimeter boundaries and therefore provide a reliable energy measurement. Electrons from photon conversions are removed with high efficiency using the tracking information in the event. A more detailed description of the primary electron selection can be found in Refs. [4,7].

The η coverage for electron detection is extended by using the plug calorimeter. When selecting plug electrons we replace the variables L_{shr}, χ^2_{strip}, Δx, and Δz used for central electrons with the χ^2 comparison of the longitudinal and transverse shower profiles, χ^2_{depth} and χ^2_{transv}, respectively. We require $\chi^2_{depth} \leq 15$ and $\chi^2_{transv} \leq 3$. We do not use the E/P cut, as the momentum measurement is not accurate at large rapidities. However, we require that a track pointing to the electromagnetic cluster has hits in at least three CTC axial layers. We also require that the ratio of the number of VTX hits found along the electron path to the predicted number be larger than 50%. Because of the CTC geometrical acceptance and of fiducial cuts to ensure a reliable energy measurement, the effective coverage for plug electrons is $1.2 \leq |\eta| \leq 1.5$.

C. Muon selection

Muons are identified in the pseudorapidity region $|\eta| \leq 1.0$ by requiring a match between a CTC track and a track segment measured by the CMU, CMP, or CMX muon cham-

bers. The following variables are used to separate muons from hadrons interacting in the calorimeter and cosmic rays: (1) an energy deposition in the electromagnetic and hadronic calorimeters characteristic of minimum ionizing particles, E_{em} and E_{had}, respectively; (2) the distance of closest approach of the reconstructed track to the beam line (impact parameter), d; (3) the z-vertex match; (4) the distance between the extrapolated track and the track segment in the muon chamber, $\Delta x = r \Delta \phi$; and (5) the isolation I. A more detailed description of the primary muon selection can be found in Refs. [4,7]. Selection efficiencies for electrons and muons in the simulation are adjusted to those of $Z \rightarrow ll$ events in the data.

D. Loose leptons

In order to be more efficient in rejecting events containing two leptons from Z decays, $t\bar{t}$ decays, and other sources we use looser selection criteria to search for additional isolated leptons. These selection criteria are described in detail in Ref. [7].

E. Jet identification and corrections

Jets are reconstructed from the energy deposited in the calorimeter using a clustering algorithm with a fixed cone of radius $R = 0.4$ in the $\eta - \phi$ space. A detailed description of the algorithm can be found in Ref. [15]. Jet energies can be mismeasured for a variety of reasons (calorimeter nonlinearity, loss of low momentum particles because of bending in the magnetic field, contributions from the underlying event, out-of-cone losses, undetected energy carried by muons and neutrinos). Corrections, which depend on the jet E_T and η, are applied to jet energies; they compensate for these mismeasurements on average but do not improve the jet energy resolution. We estimate a 10% uncertainty on the corrected jet energy [4,16]. Where appropriate, we apply additional corrections to jet energies in order to extrapolate on average to the energy of the parton producing the jet [4,17,18].

F. $\not{E}_T$ measurement

The missing transverse energy ($\not{E}_T$) is defined as the negative of the vector sum of the transverse energy in all calorimeter towers with $|\eta| \leq 3.5$. For events with muon candidates the vector sum of the calorimeter transverse energy is corrected by vectorially subtracting the energy deposited by the muon and then adding the p_T of the muon as measured by the tracking detectors. This is done for all muon candidates with $p_T \geq 5$ GeV/c and $I \leq 0.1$. When jet energy corrections are used, the $\not{E}_T$ calculation accounts for them as detailed in Ref. [17].

IV. THE $W+$JET SAMPLE

The W selection requires an isolated, $I \leq 0.1$, electron (muon) to pass the trigger and offline requisites outlined in Sec. III, and also to have $E_T \geq 20$ GeV ($p_T \geq 20$ GeV/c). We require the z position of the event vertex (Z_{vrtx}) to be within 60 cm of the center of the CDF detector. We additionally require $\not{E}_T \geq 20$ GeV to reduce the background from misidentified leptons and semileptonic b-hadron decays. Events containing additional loose lepton candidates with isolation $I \leq 0.15$ and $p_T \geq 10$ GeV/c are removed from the sample. We bin the W candidate events according to the observed jet multiplicity (a jet is a $R = 0.4$ cluster with uncorrected $E_T \geq 15$ GeV and $|\eta| \leq 2.0$).

The heavy flavor content of the $W+$jet sample is enhanced by selecting events with jets containing a displaced secondary vertex or a soft lepton.

A. Description of the tagging algorithms

The secondary vertex tagging algorithm (SECVTX) is described in detail in Refs. [4,7]. SECVTX is based on the determination of the primary event vertex and the reconstruction of additional secondary vertices using displaced tracks contained inside jets. The search for a secondary vertex in a jet is a two-stage process. In both stages, tracks in the jet are selected for the reconstruction of a secondary vertex based on the significance of their impact parameter d with respect to the primary vertex, d/σ_d, where σ_d is the estimated uncertainty on d. The first stage requires at least three candidate tracks for the reconstruction of the secondary vertex. Tracks consistent with coming from the decay $K_s \rightarrow \pi^+ \pi^-$ or $\Lambda \rightarrow \pi^- p$ are not used as candidate tracks. Two candidate tracks are constrained to pass through the same space point to form a seed vertex. If at least one additional candidate track is consistent with intersecting this seed vertex, then the seed vertex is used as the secondary vertex. If the first stage is not successful in finding a secondary vertex, a second pass is attempted. More stringent track requirements (such as d/σ_d and p_T) are imposed on the candidate tracks. All candidate tracks satisfying these stricter criteria are constrained to pass through the same space point to form a seed vertex. This vertex has an associated χ^2. Candidate tracks that contribute too much to the χ^2 are removed and a new seed vertex is formed. This procedure is iterated until a seed vertex remains that has at least two associated tracks and an acceptable value of χ^2.

The decay length of the secondary vertex L_{xy} is the projection in the plane transverse to the beam line of the vector pointing from the primary vertex to the secondary vertex onto the jet axis. If the cosine of the angle between these two vectors is positive (negative), then L_{xy} is positive (negative). Most of the secondary vertices from the decay of b and c hadrons are expected to have positive L_{xy}; conversely, secondary vertices constructed from a random combination of mismeasured tracks (mistags) have a symmetric distribution around $L_{xy} = 0$. To reduce the background, a jet is considered tagged by SECVTX if it contains a secondary vertex with $L_{xy}/\sigma_{L_{xy}} \geq 3.0$, where $\sigma_{L_{xy}}$ is the estimated uncertainty on L_{xy} (typically about 130 μm). The mistag contribution to positive SECVTX tags is evaluated using a parametrization derived from negative tags in generic-jet data [7].

A second b-tagging method is represented by the jet-probability (JPB) algorithm described in detail in Ref. [7]. This tagging method compares track impact parameters to measured resolution functions in order to calculate for each

jet a probability that there are no long-lived particles in the jet cone. The sign of the impact parameter is defined to be positive if the point of closest approach to the primary vertex lies in the same hemisphere as the jet direction, and negative otherwise. Jet probability is defined using tracks with positive impact parameter; we also define a negative jet probability where we select only tracks with negative impact parameter in the calculation. Jet probability is uniformly distributed for light quark or gluon jets, but is very small for jets containing displaced vertices from heavy flavor decays. A jet has a positive (negative) JPB tag if a jet-probability value smaller than 0.05 is derived using at least two tracks with a positive (negative) impact parameter.

An alternative way to tag b quarks is to search a jet for soft leptons produced by $b \to l\nu c$ or $b \to c \to l\nu s$ decays. The soft lepton tagging algorithm is applied to sets of CTC tracks associated with jets with $E_T \geq 15$ GeV and $|\eta| \leq 2.0$. The CTC tracks are associated with a jet if they are inside a cone of radius 0.4 centered around the jet axis. In order to maintain high efficiency, the lepton p_T threshold is set low at 2 GeV/c.

To search for soft electrons the algorithm extrapolates each track to the calorimeter and attempts to match it to a CES cluster. The matched CES cluster is required to be consistent in shape and position with the expectation for electron showers. In addition, it is required that $0.7 \leq E/P \leq 1.5$ and $E_{had}/E_{em} \leq 0.1$. The track specific ionization (dE/dx), measured in the CTC, is required to be consistent with the electron hypothesis. Electron candidates must also have an energy deposition in the CPR corresponding to that left by at least four minimum-ionizing particles. The efficiency of the selection criteria has been determined using a sample of electrons produced by photon conversions [4].

To identify soft muons, track segments reconstructed in the CMU, CMP, or CMX systems are matched to the CTC tracks. Only the CMU or CMX systems are used to identify muons with $2 \leq p_T \leq 3$ GeV/c. Muon candidate tracks with $p_T \geq 3$ GeV/c within the CMU and CMP fiducial volume are required to match to track segments in both systems. The reconstruction efficiency has been measured using samples of muons from $J/\psi \to \mu^+\mu^-$ and $Z \to \mu^+\mu^-$ decays [4].

In the data the rate of fake soft lepton tags which are not due to heavy flavor semileptonic decays is evaluated using a parametrization of the SLT fake probability per track as a function of the track isolation and p_T. This parametrization has been derived in a large sample of generic-jet data [4] after removing the fraction of soft lepton tags contributed by heavy flavor (about 26%) [7]. In the simulation, a SLT track is required to match at generator level a lepton coming from a b or c-hadron decay [7].

B. Monte Carlo generators and detector simulation

We use three different Monte Carlo generators to estimate the contribution of SM processes to the $W+$jet sample. The settings and the calibration of these Monte Carlo generators are described in Ref. [7].

A few processes, including $t\bar{t}$ production, are evaluated using version 5.7 of PYTHIA [19]. These processes are detailed in the next section.

The fraction of $W+$jet direct production with heavy flavor, namely $p\bar{p} \to Wg$ with $g \to b\bar{b}, c\bar{c}$ (gluon splitting) and $p\bar{p} \to Wc$, is calculated using version 5.6 of the HERWIG generator [20]. The part of the phase space region of these hard scattering processes that is not correctly mapped by HERWIG (namely $Wb\bar{b}$ and $Wc\bar{c}$ events in which the two heavy flavor partons produce two well separated jets) is evaluated using the VECBOS generator [21]. VECBOS is a parton-level Monte Carlo generator and we transform the partons produced by VECBOS into hadrons and jets using HERWIG adapted to perform the coherent shower evolution of both initial and final state partons from an arbitrary hard-scattering subprocess [22]. In summary, we use HERWIG to predict the fraction of $W+ \geq 1$ jet events where only one jet contains b or c hadrons while we rely on VECBOS to extend the prediction to the cases where two different jets contain heavy-flavored hadrons. The Martin-Roberts-Stirling (MRS) D_0' set of structure functions [23] is used with these generators. We set the b-mass value to 4.75 GeV/c^2 and the c-mass value to 1.5 GeV/c^2.

The fraction of jets containing heavy flavor hadrons from gluon splitting predicted by the Monte Carlo generators has been tuned using generic-jet data. As a result, the fraction of $g \to b\bar{b}$ calculated by the generators is increased by the factor 1.40 ± 0.19 and the fraction of $g \to c\bar{c}$ by the factor 1.35 ± 0.36. These factors are of the same size as those measured by the SLAC Linear Collider (SLC) and CERN e^+e^- collider (LEP) experiments for the rate of $g \to b\bar{b}$ and $g \to c\bar{c}$ in Z decays [24], and are within the estimated theoretical uncertainties [25].

We use the CLEO Monte Carlo generator, QQ, to model the decay of b and c hadrons [26]. All particles produced in the final state by the HERWIG (or PYTHIA) + QQ generator package are decayed and interacted with the CDF-detector simulation (called QFL). The detector response is based upon parametrizations and simple models which depend on the particle kinematics. After the simulation of the CDF detector, the Monte Carlo events are treated as if they were real data. Reference [7] describes the calibration of the detector simulation, including tagging efficiencies, using several independent data samples.

V. COMPARISON OF MEASURED AND PREDICTED RATES OF $W+ \geq 1$ JET EVENTS WITH HEAVY FLAVOR TAGS

In this study we compare the observed numbers of tagged $W+$jet events as a function of the jet multiplicity to the SM prediction which uses the next-to-leading order (NLO) calculation of the $t\bar{t}$ cross section. The various contributions to $W+$jet events are discussed in Sec. V A, and the results of the comparisons are summarized in Sec. V B.

A. Predicted contributions to the $W+$jet event sample

A detailed study of the non-$t\bar{t}$ contributions to the $W+$jet events was made in Ref. [7]. These studies are reviewed here, along with the $t\bar{t}$ contribution derived using the theoretical prediction.

TABLE I. Estimated composition of the $W+\geq 1$ jet sample before tagging.

Source	$W+1$ jet	$W+2$ jet	$W+3$ jet	$W+\geq 4$ jet
Data	9454	1370	198	54
Non-W	560.1 ± 14.9	71.2 ± 2.7	12.4 ± 2.0	5.1 ± 1.7
WW	31.2 ± 5.4	31.1 ± 5.4	5.2 ± 1.0	0.8 ± 0.2
WZ	4.4 ± 0.9	4.8 ± 1.0	0.9 ± 0.2	0.1 ± 0.0
ZZ	0.3 ± 0.1	0.4 ± 0.1	0.1 ± 0.0	0.0 ± 0.0
Unidentified-$Z+$jets	234.8 ± 14.5	38.5 ± 5.9	7.9 ± 2.4	0.7 ± 0.7
Single top	14.1 ± 2.1	7.9 ± 1.7	1.7 ± 0.4	0.3 ± 0.1
$t\bar{t}$	1.8 ± 0.5	10.1 ± 2.8	20.3 ± 5.7	21.3 ± 5.9
$W+$jets without h.f.	7952.0 ± 133.6	1027.7 ± 31.1	121.1 ± 7.7	19.9 ± 6.1
Wc	413.1 ± 123.9	86.8 ± 26.1	11.2 ± 3.4	1.9 ± 0.7
$Wc\bar{c}$	173.1 ± 46.2	61.9 ± 13.6	11.4 ± 2.6	2.3 ± 0.9
$Wb\bar{b}$	69.0 ± 9.5	29.7 ± 5.1	5.7 ± 1.1	1.5 ± 0.5

The small number of events contributed by non-W sources, including $b\bar{b}$ production, is estimated using the data. The number of non-W events in the signal region (lepton $I\leq 0.1$ and $\not{E}_T\geq 20\,\mathrm{GeV}$) is predicted by multiplying the number of events with $I\leq 0.1$ and $\not{E}_T\leq 10\,\mathrm{GeV}$ by the ratio R of events with $I\geq 0.2$ and $\not{E}_T\geq 20\,\mathrm{GeV}$ to events with $I\geq 0.2$ and $\not{E}_T\leq 10\,\mathrm{GeV}$. The number of tagged non-W events is predicted by multiplying the number of tagged events with $I\leq 0.1$ and $\not{E}_T\leq 10\,\mathrm{GeV}$ by the same ratio R.

The number of $Z+$jet events in which one lepton from the Z decay is not identified (unidentified-Z) is calculated using the PYTHIA generator. The simulated sample is normalized to the number of $Z\to ll$ decays observed in the data for each jet bin. Unidentified-$Z+$jet events can be tagged either because a jet is produced by a τ originating from $Z\to\tau\bar{\tau}$ decays or because a jet contains heavy flavor. The number of tagged $Z\to\tau\bar{\tau}$ events is estimated using the PYTHIA simulation. The number of tags contributed by unidentified-$Z+$jet events with heavy flavor is estimated with a combination of the PYTHIA, HERWIG, and VECBOS generators.

The contribution of diboson production before and after tagging is calculated using the PYTHIA generator. The values of the diboson production cross sections [$\sigma_{WW}=9.5\pm 0.7$ pb, $\sigma_{WZ}=2.60\pm 0.34$ pb, and $\sigma_{ZZ}=1.0\pm 0.2$ pb] are taken from Ref. [27].

The contribution from single top production before and after tagging is estimated using PYTHIA to model the process $p\bar{p}\to t\bar{b}$ via a virtual s-channel W and HERWIG to model the process $p\bar{p}\to t\bar{b}$ via a virtual t-channel W. The production cross sections [0.74 ± 0.05 pb and 1.5 ± 0.4 pb for the s and t channel, respectively] are derived using the NLO calculation of Ref. [28].

The $t\bar{t}$ contribution is calculated using the PYTHIA generator. We use $\sigma_{t\bar{t}}=5.1$ pb with a 15% uncertainty. This number is the average of several NLO calculations of the $t\bar{t}$ production cross section [8].

The direct production of $W+$jets with heavy flavor is estimated using a combination of data and simulation. Since the leading-order matrix element calculation has a 40% un-certainty [29], we first evaluate in each jet bin the number of events due to $W+$jet direct production as the difference between the data and the sum of all processes listed above, including $t\bar{t}$ production, before tagging. We then use the HERWIG and VECBOS generators, calibrated with generic-jet data as discussed in Sec. IV B, to estimate the fraction of $W+$jet events which contain $c\bar{c}$ or $b\bar{b}$ pairs and their tag contribution. The fraction of Wc events and their tag contribution is determined using HERWIG.

The number of events in which a jet without heavy flavor (h.f.) is tagged because of detector effects (mistags) is estimated using a parametrization of the mistag probability (as a function of the jet transverse energy and track multiplicity), which has been derived from generic-jet data.

B. Comparison with a SM prediction using the theoretical estimate of $\sigma_{t\bar{t}}$

The composition of the $W+$jet event candidates before heavy flavor tagging is summarized in Table I. As previously discussed in Sec. IV A, the heavy flavor content of the $W+$jet sample is enriched by searching jets for a displaced secondary vertex (SECVTX tag) or an identified lepton (SLT tag).

The composition of the $W+$jet events with SECVTX tags is shown in Table II and those with SLT tags in Table III. The numbers of observed events with one [single tag (ST)] or two [double tag (DT)] jets tagged by the SECVTX or SLT algorithms are compared to predictions for each value of the jet multiplicity.

There is good agreement between the observed and predicted numbers of tagged events for the four jet multiplicity bins. The probability [30] that the observed numbers of events with at least one SECVTX tag are consistent with the predictions in all four jet bins is 80%. The probability [30] that the observed number of events with at least one SLT tag are consistent with the predictions in all four jet bins is 56%.

In the next section we perform a more detailed study of the heavy flavor content of the $W+$jet sample by selecting

TABLE II. Summary of observed and predicted number of W events with one (ST) and two (DT) SECVTX tags.

Source	$W+1$ jet	$W+2$ jet	$W+3$ jet	$W+\geqslant 4$ jet
Mistags	10.82 ± 1.08	3.80 ± 0.38	0.99 ± 0.10	0.35 ± 0.04
Non-W	8.18 ± 0.78	1.49 ± 0.47	0.76 ± 0.38	0.31 ± 0.16
WW,WZ,ZZ	0.52 ± 0.14	1.38 ± 0.28	0.40 ± 0.13	0.00 ± 0.00
Single top	1.36 ± 0.35	2.38 ± 0.54	0.63 ± 0.14	0.14 ± 0.03
Wc	16.89 ± 5.38	3.94 ± 1.30	0.51 ± 0.17	0.09 ± 0.04
$Wc\bar{c}$ (ST)	7.89 ± 2.17	3.54 ± 0.88	0.77 ± 0.25	0.16 ± 0.07
$Wc\bar{c}$ (DT)		0.06 ± 0.04	0.00 ± 0.00	0.00 ± 0.00
$Wb\bar{b}$ (ST)	17.00 ± 2.41	8.35 ± 1.74	1.62 ± 0.40	0.41 ± 0.14
$Wb\bar{b}$ (DT)		1.51 ± 0.52	0.31 ± 0.13	0.07 ± 0.03
$Z\rightarrow\tau\tau$	0.96 ± 0.30	0.70 ± 0.25	0.17 ± 0.12	0.00 ± 0.00
Zc	0.14 ± 0.04	0.03 ± 0.01	0.01 ± 0.00	0.00 ± 0.00
$Zc\bar{c}$ (ST)	0.22 ± 0.06	0.10 ± 0.03	0.04 ± 0.02	0.00 ± 0.00
$Zc\bar{c}$ (DT)		0.00 ± 0.00	0.00 ± 0.00	0.00 ± 0.00
$Zb\bar{b}$ (ST)	0.93 ± 0.14	0.46 ± 0.12	0.17 ± 0.06	0.02 ± 0.02
$Zb\bar{b}$ (DT)		0.08 ± 0.03	0.03 ± 0.02	0.00 ± 0.00
$t\bar{t}$ (ST)	0.54 ± 0.14	3.34 ± 0.87	6.76 ± 1.76	7.42 ± 1.93
$t\bar{t}$ (DT)		0.76 ± 0.20	2.88 ± 0.75	3.96 ± 1.03
SM prediction (ST)	65.44 ± 6.45	29.61 ± 2.66	12.87 ± 1.89	8.92 ± 1.95
SM prediction (DT)		2.41 ± 0.56	3.23 ± 0.76	4.03 ± 1.03
Data (ST)	66	35	10	11
Data (DT)		5	6	2

events with jets containing both a displaced vertex and a soft lepton.

VI. COMPARISON OF MEASURED AND PREDICTED RATES OF $W+$JET EVENTS WITH BOTH A SECVTX AND SLT HEAVY FLAVOR TAG

We begin this study by selecting $W+$jet events with both SECVTX and SLT tags. In Table IV the predicted and observed $W+$jet events with a SLT tag are split into samples without (top part of Table IV) and with (bottom part of Table IV) SECVTX tags. There is good agreement between data and predictions for the $W+$jet events with a SLT tag and no SECVTX tag, where a large fraction of the events have fake SLT tags in jets without heavy flavor. In contrast, the numbers of events with both SECVTX and SLT tags, which are mostly contributed by real heavy flavor, are not well predicted by the simulation. Therefore, we check if the rate of SLT tags in jets tagged by SECVTX (superjets) is consistent with the expected production and decay of hadrons with heavy flavor.

After tagging with SECVTX, we estimate that approximately 70% of the $W+$jet sample contains b jets and 20% contains c jets (see Table II). On average, 20% of the b- and c-hadron decays produce a lepton (e or μ). Only 50% of the leptons resulting from a b-hadron satisfy the 2 GeV/c transverse momentum requirement of the soft lepton tag (this fraction is slightly smaller for c-hadron decays). In addition, the SLT tagger is approximately 90% efficient in identifying

muons and 50% efficient in identifying electrons. Altogether, we then expect that about 7% of the jets tagged by SECVTX will contain an additional SLT tag if the heavy flavor composition of $W+$jet events is correctly understood.

The observed numbers of events with a superjet are compared to the SM prediction in Table V. The information in Table V is similar to that presented in Table IV, except that two events listed in Table IV have the SLT and SECVTX tags in different jets. The probability [30] that the observed numbers of events with at least one superjet are consistent with the prediction in all four jet bins is 0.4%. This low probability value is mostly driven by an excess in the $W+2,3$ jet bins where 13 events are observed[2] and 4.4 ± 0.6 are expected from SM sources. The *a posteriori* probability of observing no less than 13 events is 0.1%. The probability for observing this excess of $W+2,3$ jet events with a superjet does not take into account the number of comparisons made in our studies in various jet-multiplicity bins and using different tagging algorithms. It is not possible to quantify precisely the effect of this "trial factor." We have carried out several statistical tests using different combinations of the observed and predicted numbers of single and double tags reported in Tables II through V. These combinations always

---

[2]The 13 events include $t\bar{t}$ candidates and four of these events are included in the sample used to measure the top quark mass [18] (see also Appendix B).

TABLE III. Summary of observed and predicted number of W events with one (ST) and two (DT) SLT tags.

Source	$W+1$ jet	$W+2$ jet	$W+3$ jet	$W+\geq 4$ jet
Mistags	101.92 ± 10.19	30.90 ± 3.09	7.34 ± 0.73	3.01 ± 0.30
Non-W	8.96 ± 0.84	2.09 ± 0.56	0.38 ± 0.27	0.16 ± 0.11
WW,WZ,ZZ	0.50 ± 0.16	0.88 ± 0.22	0.10 ± 0.05	0.00 ± 0.00
Single top	0.38 ± 0.10	0.67 ± 0.15	0.18 ± 0.05	0.05 ± 0.01
Wc	13.12 ± 4.27	4.29 ± 1.46	0.73 ± 0.32	0.13 ± 0.06
$Wc\bar{c}$ (ST)	6.41 ± 1.89	2.70 ± 0.67	0.69 ± 0.22	0.14 ± 0.06
$Wc\bar{c}$ (DT)		0.02 ± 0.02	0.00 ± 0.00	0.00 ± 0.00
$Wb\bar{b}$ (ST)	5.31 ± 0.96	2.86 ± 0.67	0.47 ± 0.14	0.12 ± 0.05
$Wb\bar{b}$ (DT)		0.09 ± 0.05	0.01 ± 0.01	0.00 ± 0.00
$Z\rightarrow\tau\tau$	0.43 ± 0.20	0.09 ± 0.09	0.09 ± 0.09	0.00 ± 0.00
Zc	0.11 ± 0.04	0.04 ± 0.01	0.01 ± 0.01	0.00 ± 0.00
$Zc\bar{c}$ (ST)	0.17 ± 0.05	0.08 ± 0.02	0.03 ± 0.01	0.00 ± 0.00
$Zc\bar{c}$ (DT)		0.00 ± 0.00	0.00 ± 0.00	0.00 ± 0.00
$Zb\bar{b}$ (ST)	0.29 ± 0.06	0.16 ± 0.04	0.05 ± 0.02	0.01 ± 0.01
$Zb\bar{b}$ (DT)		0.00 ± 0.00	0.00 ± 0.00	0.00 ± 0.00
$t\bar{t}$	0.14 ± 0.06	1.35 ± 0.61	2.85 ± 1.30	3.36 ± 1.53
$t\bar{t}$ (DT)		0.04 ± 0.02	0.13 ± 0.06	0.18 ± 0.08
SM prediction (ST)	137.75 ± 11.29	46.08 ± 3.65	12.91 ± 1.57	6.98 ± 1.57
SM prediction (DT)		0.14 ± 0.06	0.14 ± 0.06	0.18 ± 0.08
Data (ST)	146	56	17	8
Data (DT)		0	0	0

include the observed numbers of supertags. We have used both a likelihood method [30] and other statistical techniques, which combine the probabilities of observing a number of tagged events at least as large as the data. These studies yield probabilities in the range of one to several percent.

The cause of the excess of $W+2,3$ jet events with supertags could be a discrepancy in the correlation between the SLT and SECVTX efficiencies in the data and simulation. These simulated efficiencies have been tuned separately using the data and, in principle, the SLT tagging efficiency in jets already tagged by SECVTX could be higher in the data than in the simulation. We have checked this using generic-jet data (see Appendix A) and we conclude that the excess of $W+2,3$ jet events with a supertag cannot be explained by this type of simulation deficiency.

VII. PROPERTIES OF THE EVENTS WITH A SUPERJET

Having observed an excess of $W+2,3$ jet events with a supertag, we next compare the kinematics of these events with the SM simulation. We check the simulation using a complementary $W+2,3$ jet sample of data. This sample is described in Sec. VII A. In Sec. VII B we compare the heavy flavor content of the additional jets in events with a superjet and in the complementary sample. In Secs. VII C and VII D we compare several kinematical distributions of these events to the simulation.

A. Complementary data sample

We check our simulation by studying a larger data sample consisting of $W+2,3$ jet events with a SECVTX tag, but no supertags. The number of observed and predicted events are compared in Table VI (43 $W+2,3$ jet events are observed, in agreement with the SM prediction of 43.6 ± 3.3). We have chosen this sample because, as shown by the comparison of Table VI with Table V, its composition is quite similar to $W+$ jet events with a supertag.[3] In order to have a complementary sample of data with the same kinematical acceptance of the events with a supertag, we also require that at least one of the jets tagged by SECVTX contains a soft lepton candidate track. After this additional requirement this sample of $W+2,3$ jet events consists of 42 events (the SM prediction is 41.2 ± 3.1 events). We note that, while closely related, this event sample has still a few features which are different from the superjet sample. For instance, most of the superjets are expected to be produced by heavy flavor semileptonic decays, in which the corresponding neutrino escapes detection, while in the complementary sample SECVTX tagged jets are predominantly produced by purely hadronic decays of heavy flavors. However, according to the simula-

---

[3]$W+2,3$ jet events with a SLT tag and no supertags are another larger statistics data set; however, the heavy flavor composition is quite different from that expected for events with a superjet.

TABLE IV. Summary of observed and predicted number of W events with a soft lepton tag. The data sample is split in events with and without SECVTX tags.

Source	$W+1$ jet	$W+2$ jet	$W+3$ jet	$W+\geq 4$ jet
Events without SECVTX tags				
Data	9388	1330	182	41
SLT mistags in $W+$jet without h.f.	93.31 ± 9.33	24.81 ± 2.48	4.74 ± 0.47	1.26 ± 0.13
Non-W	8.39 ± 0.67	1.67 ± 0.44	0.31 ± 0.22	0.13 ± 0.09
WW,WZ,ZZ	0.83 ± 0.15	1.58 ± 0.21	0.31 ± 0.04	0.05 ± 0.00
Single top	0.27 ± 0.06	0.46 ± 0.09	0.13 ± 0.03	0.03 ± 0.01
Wc	16.97 ± 4.08	5.99 ± 1.40	1.10 ± 0.30	0.22 ± 0.06
$Wc\bar{c}$	7.99 ± 1.81	3.78 ± 0.51	1.02 ± 0.39	0.25 ± 0.12
$Wb\bar{b}$	4.47 ± 0.68	2.26 ± 0.43	0.31 ± 0.07	0.10 ± 0.03
$Z\to\tau\tau$	0.83 ± 0.20	0.40 ± 0.09	0.15 ± 0.09	0.02 ± 0.00
Zc	0.14 ± 0.03	0.05 ± 0.01	0.02 ± 0.01	0.00 ± 0.00
$Zc\bar{c}$	0.22 ± 0.05	0.11 ± 0.03	0.05 ± 0.02	0.01 ± 0.00
$Zb\bar{b}$	0.23 ± 0.04	0.11 ± 0.03	0.03 ± 0.01	0.00 ± 0.00
$t\bar{t}$	0.11 ± 0.05	0.85 ± 0.31	1.90 ± 0.65	2.15 ± 0.69
SM prediction	133.75 ± 10.38	42.06 ± 2.99	10.06 ± 0.98	4.22 ± 0.72
Data with SLT tags	145	47	12	5
Events with SECVTX tags				
Data	66	40	16	13
SECVTX mistags in events with SLT tags	0.28 ± 0.03	0.20 ± 0.02	0.16 ± 0.02	0.05 ± 0.01
Non-W	0.57 ± 0.05	0.42 ± 0.11	0.08 ± 0.05	0.03 ± 0.02
WW,WZ,ZZ	0.02 ± 0.02	0.16 ± 0.03	0.03 ± 0.01	0.00 ± 0.00
Single top	0.12 ± 0.04	0.32 ± 0.06	0.09 ± 0.02	0.02 ± 0.01
Wc	0.88 ± 0.29	0.38 ± 0.12	0.17 ± 0.02	0.02 ± 0.00
$Wc\bar{c}$	0.41 ± 0.13	0.41 ± 0.13	0.14 ± 0.05	0.03 ± 0.01
$Wb\bar{b}$	1.58 ± 0.33	1.40 ± 0.30	0.40 ± 0.08	0.11 ± 0.02
$Z\to\tau\tau$	0.00 ± 0.00	0.00 ± 0.00	0.00 ± 0.00	0.00 ± 0.00
Zc	0.01 ± 0.00	0.00 ± 0.00	0.00 ± 0.00	0.00 ± 0.00
$Zc\bar{c}$	0.01 ± 0.00	0.01 ± 0.00	0.01 ± 0.00	0.00 ± 0.00
$Zb\bar{b}$	0.08 ± 0.02	0.06 ± 0.02	0.03 ± 0.01	0.01 ± 0.00
$t\bar{t}$	0.04 ± 0.02	0.78 ± 0.30	1.88 ± 0.65	2.65 ± 0.85
SM prediction	4.00 ± 0.47	4.15 ± 0.50	2.99 ± 0.66	2.93 ± 0.85
Data with SECVTX and SLT tags	1	9	5	3

tion, a large fraction of heavy flavor semileptonic decays is not identified by the SLT algorithm and is also included in the complementary sample. All such effects are in principle described by the simulation.

B. Heavy flavor content of additional jets

The heavy flavor content of the second and third jet in the events can be inferred from the rate of additional SECVTX tags. Tables V and VI show the number of observed and predicted events with an additional jet tagged by SECVTX in superjet events and in the complementary sample. In the latter data sample, in which according to the simulation in Table VI most of the events contain a second jet with b

flavor, there are 6 $W+2,3$ jet events with a double SECVTX tag, in agreement with the expectation of 5.02 ± 0.84 events.

Of the 13 $W+2,3$ jet events with a superjet five contain an additional SECVTX tag. If the 13 events are a fluctuation of SM processes, we expect to find 1.8 ± 0.3 events with a double tag.[4] The probability of observing five or more $W+2,3$ jet events with double tags is 4.1%. Given the high probability of finding an additional SECVTX tag, we apply b-jet specific energy corrections to the additional jets in the event. These jets are later referred to as "b jets."

---

[4]The prediction is 0.62 ± 0.10 events with a double tag in 4.4 events with a superjet.

TABLE V. Observed and predicted number of W+jet events with a supertag. The subsample of events with an additional SECVTX tag (DT) is also listed.

Source	$W+1$ jet	$W+2$ jet	$W+3$ jet	$W+\geqslant4$ jet
SECVTX mistags in events with SLT tags	0.28 ± 0.03	0.09 ± 0.01	0.07 ± 0.01	0.02 ± 0.00
Non-W	0.57 ± 0.05	0.13 ± 0.03	0.00 ± 0.00	0.00 ± 0.00
WW,WZ,ZZ	0.02 ± 0.02	0.13 ± 0.06	0.01 ± 0.01	0.00 ± 0.00
Single top	0.12 ± 0.04	0.24 ± 0.05	0.07 ± 0.02	0.02 ± 0.00
Wc	0.88 ± 0.29	0.24 ± 0.14	0.14 ± 0.10	0.00 ± 0.00
$Wc\bar{c}$	0.41 ± 0.13	0.25 ± 0.09	0.13 ± 0.06	0.00 ± 0.00
$Wb\bar{b}$	1.58 ± 0.33	1.07 ± 0.26	0.19 ± 0.09	0.01 ± 0.00
$Z\rightarrow\tau\tau$	0.00 ± 0.00	0.00 ± 0.00	0.00 ± 0.00	0.00 ± 0.00
Zc	0.01 ± 0.00	0.00 ± 0.00	0.00 ± 0.00	0.00 ± 0.00
$Zc\bar{c}$	0.01 ± 0.00	0.01 ± 0.00	0.01 ± 0.00	0.00 ± 0.00
$Zb\bar{b}$	0.08 ± 0.02	0.05 ± 0.02	0.02 ± 0.01	0.00 ± 0.00
$t\bar{t}$	0.04 ± 0.02	0.48 ± 0.19	1.08 ± 0.40	1.42 ± 0.49
SM prediction (supertags)	4.00 ± 0.50	2.69 ± 0.41	1.71 ± 0.40	1.47 ± 0.51
SM prediction (DT)		0.26 ± 0.06	0.36 ± 0.08	0.50 ± 0.13
Data (supertags)	1	8	5	2
Data (DT)		2	3	0

C. Method for testing if the data are consistent with the SM simulation

In Sec. VII D we study distributions of several simple kinematic variables x_i for the 13 events with a superjet and the complementary sample of 42 events. Each data distribution is compared with the sum of the 12 SM contributions, $SM_j(x_i)$, listed in Tables V and VI using a Kolmogorov-Smirnov (KS) test [31,32]. Using the cumulative distribution functions $F(x_i)$ and $H(x_i)$ of the two distributions to be compared, the KS distance is defined as $\delta=\max[F(x_i)-H(x_i)]+\max[H(x_i)-F(x_i)]$. This is Kuiper's definition of the KS distance [33].

For each variable x_i, the probability distribution of the KS distance, $W_i(\delta)$, is determined with Monte Carlo pseudoexperiments. In each experiment, we randomly generate parent distributions $\Sigma_{j=1}^{12}(\mathcal{I}_j^r/\mathcal{I}_j)SM_j(x_i)$ for two and three jet events independently. The integral $\mathcal{I}_j=\int SM_j(x_i)dx_i$ corresponds to the average number of events contributed by the

TABLE VI. Observed and predicted number of W+jet events tagged by SECVTX after removing events with a supertag. The subsample of events with an additional SECVTX tag (DT) is also listed.

Source	$W+1$ jet	$W+2$ jet	$W+3$ jet	$W+\geqslant4$ jet
Mistags	10.52 ± 1.00	3.72 ± 0.34	0.93 ± 0.09	0.34 ± 0.04
Non-W	7.61 ± 0.06	1.36 ± 0.04	0.76 ± 0.03	0.31 ± 0.03
WW,WZ,ZZ	0.50 ± 0.14	1.25 ± 0.25	0.40 ± 0.13	0.00 ± 0.00
Single top	1.24 ± 0.31	2.15 ± 0.49	0.56 ± 0.13	0.12 ± 0.03
Wc	16.02 ± 5.13	3.70 ± 1.29	0.37 ± 0.13	0.09 ± 0.03
$Wc\bar{c}$	7.48 ± 2.08	3.35 ± 0.86	0.64 ± 0.22	0.16 ± 0.06
$Wb\bar{b}$	15.42 ± 2.21	8.80 ± 1.63	1.74 ± 0.40	0.47 ± 0.13
$Z\rightarrow\tau\tau$	0.96 ± 0.30	0.70 ± 0.25	0.17 ± 0.12	0.00 ± 0.00
Zc	0.13 ± 0.04	0.03 ± 0.01	0.01 ± 0.00	0.00 ± 0.00
$Zc\bar{c}$	0.21 ± 0.06	0.10 ± 0.03	0.03 ± 0.02	0.00 ± 0.00
$Zb\bar{b}$	0.85 ± 0.13	0.48 ± 0.11	0.19 ± 0.06	0.02 ± 0.02
$t\bar{t}$	0.50 ± 0.16	3.62 ± 1.00	8.56 ± 2.38	9.96 ± 2.40
SM prediction	61.44 ± 6.09	29.26 ± 2.58	14.39 ± 2.34	11.48 ± 2.37
SM prediction (DT)		2.15 ± 0.50	2.87 ± 0.67	3.53 ± 0.90
Data	65	32	11	11
Data (DT)		3	3	2

process j and, in each pseudoexperiment, the value $\mathcal{I}_j^r$ accounts for Poisson fluctuations and Gaussian uncertainties in $\mathcal{I}_j$. We use these parent distributions to randomly generate the same number of x_i values as in the data, but we evaluate the KS distance of the x_i distribution in each pseudoexperiment with respect to the parent distribution $\Sigma_{j=1}^{12} SM_j(x)$. Using the so derived $W_i(\delta)$ distribution, we define the probability P_i that the x_i distribution of the data is consistent with the SM simulation as $P_i = \int_{\delta_i^0}^{\infty} W_i(\delta) d\delta$, where δ^0 is the KS distance of the data.

D. Comparison of kinematical distributions in the data with the SM simulation

We test if the events with a superjet are consistent with the SM prediction by comparing the production cross sections $d^2\sigma/dp_T d\eta$ of each object in the final state. In all SM processes contributing to these events, these differential cross sections approximately factorize, and $d^2\sigma/dp_T d\eta \simeq f(p_T) \cdot g(\eta)$. Therefore we compare data and SM simulation in the following kinematical variables: the transverse energy and pseudorapidity distributions of the primary leptons, the superjets, the additional jets in the event (referred to as b jets), and the neutral object producing the missing energy in the event.[5] The kinematics of the neutral object producing the missing energy cannot be measured directly. However, correlated quantities are the transverse energy and the rapidity of the recoiling system $l+b+suj$ composed of the primary lepton (l), the superjet (suj), and each additional jet (b) in the event. Since the total transverse momentum of the events is conserved, in $W+2$ jet events the transverse energy $E_T^{l+b+suj}$ of the system $l+b+suj$ is a measure of the missing transverse energy. In the rest frame of the initial state partons producing $W+2$ jet events, the rapidities of the system $l+b+suj$ and of the object producing the missing energy are also correlated. This correlation is, however, smeared by the unknown Lorentz boost of the initial parton system. For uniformity, in $W+3$ jet events we use the same variables with two entries per event (corresponding to the two possible choices for the b jet).

We finally test the distribution of the azimuthal angle $\delta\phi^{l,b+suj}$ between the primary lepton and the system $b+suj$ composed by the superjet and each additional b jet with the purpose of checking if the events are consistent with the simulated production and decay of W bosons. The W transverse mass can be described with the variables E_T^l and $\not{E}_T$, which are already used, and the azimuthal angle between the primary lepton and the W direction. Since the total transverse momentum of the events is conserved, in $W+2$ jet events this azimuthal angle can be inferred from the supplementary angle $\delta\phi^{l,b+suj}$. For uniformity, in $W+3$ jet events we use the same variable with two entries per event.

This minimal set of nine variables is sufficient to describe the kinematics of the final state with relatively modest cor-

---

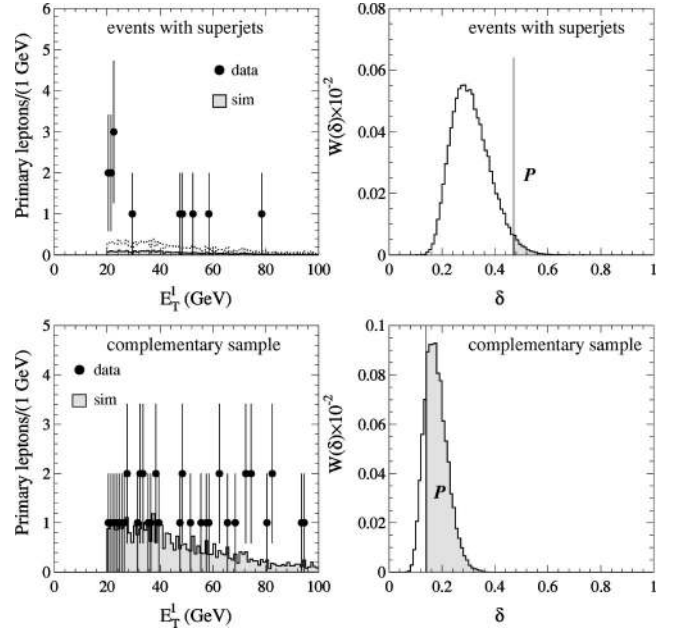[5]Jet energies are corrected using the full set of correction functions developed to measure the top mass [4,17,18].

FIG. 1. Distributions of the transverse energy of the primary lepton for the data (•) are compared to the SM prediction (shaded histograms). The dotted histograms show the SM simulation normalized to the data. The probability distribution of the KS distance δ is calculated with Monte Carlo pseudoexperiments (see text). The vertical line indicates the observed distance δ^0 between the cumulative distributions of the data and the simulation. The integral of the shaded area represents the probability P of measuring a KS distance no smaller than δ^0.

relations. The observed and predicted distributions of these kinematical variables are compared in Figs. 1–9. For each comparison, we show the probability P that the data are consistent with the simulation. Table VII summarizes the probabilities of these comparisons. The SM simulation models correctly the complementary sample of data, but has a systematically low probability of being consistent with the kinematical distributions of the events with a superjet.

In addition, one notices that the rapidity distributions of the primary lepton and the jets in the 13 events (Figs. 2, 4, 6, and 8) are not symmetric around $\eta=0$ and are more populated at positive rapidities. These observations led to additional investigations of the characteristics of the 13 events exploring the possibility that some detector effects were not properly modeled by the simulation. These studies have not revealed any anomaly which could be taken as an indication of detector problems. In particular, asymmetries due to detector problems are not visible in the complementary sample nor in the larger statistics sample of generic-jet data. However, as shown in Fig. 10, we discovered that the primary vertex of these events has an asymmetric z distribution (z is the axis along the beam line). Again, such an asymmetry is not observed in any of the large statistics data samples available. The binomial probability of observing an equal or larger asymmetry due to a statistical fluctuation in the distribution of the event vertex is 1.1%. Similar probabilities for the asymmetry in several rapidity distributions are in the range between 1.5% to 10%. Since we know of no physics
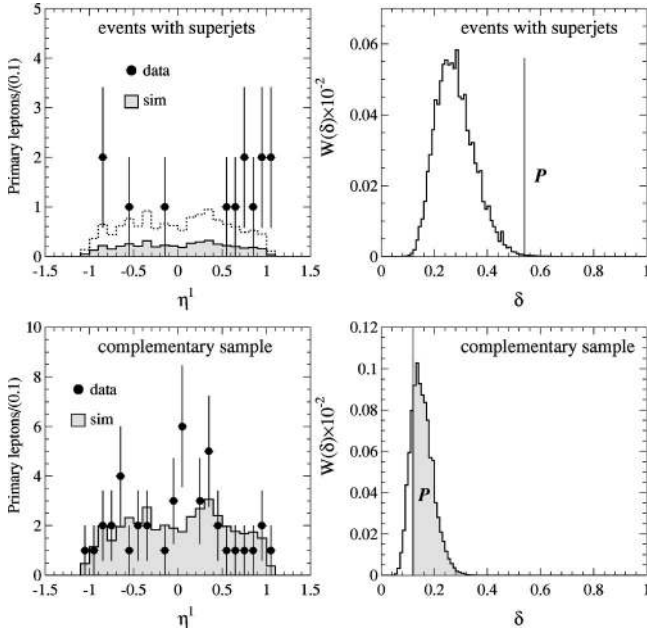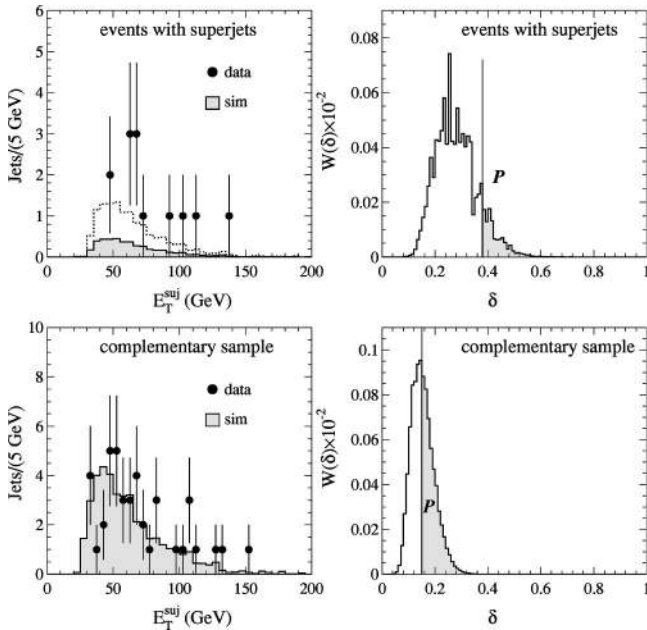
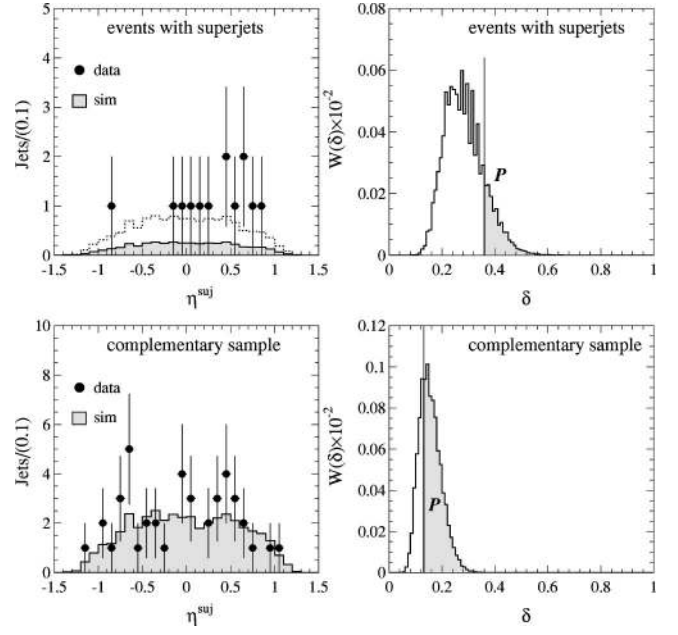FIG. 2. Distribution of the pseudorapidity of the primary lepton in events with a superjet and in the complementary sample.

FIG. 4. Distribution of the pseudorapidity of the superjet in events with a superjet and in the complementary sample.

process that would produce such asymmetries, it is possible that an obscure detector problem, not seen in other samples, is responsible; or it may be that these asymmetries are due to a low probability statistical fluctuation.

The set of nine kinematic variables used to compare data and simulation is not the only possible choice. We also looked at nine complementary variables, and Table VIII shows the result of the KS test for this set of kinematic distributions: $\not{E}_T$, the corrected transverse missing energy; M_T^W, the W transverse mass calculated using the primary

lepton and $\not{E}_T$; M^{b+suj}, y^{b+suj}, and E_T^{b+suj}, the invariant mass, rapidity, and transverse energy of the system $b+suj$, respectively; $M^{l+b+suj}$, the invariant mass of the system $l+b+suj$; $\delta\theta^{b,suj}$ and $\delta\phi^{b,suj}$, the angle and the azimuthal angle between the superjet and the b jets, respectively; and $\delta\theta^{l,b+suj}$, the angle between the primary lepton and the system $b+suj$. The simulation correctly models these distributions for the complementary sample, while the probabilities for events with a superjet are systematically lower. However, the disagreement between events with a superjet and their
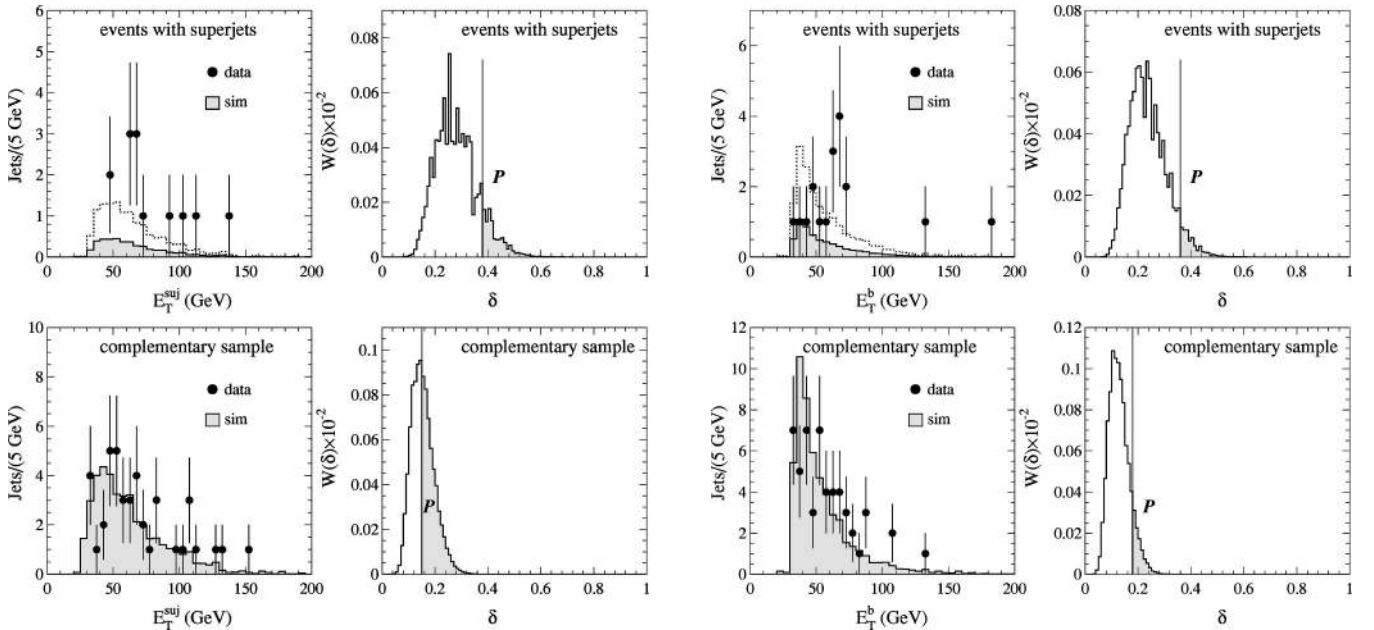

FIG. 3. Distribution of the transverse energy of the superjet in events with a superjet and in the complementary sample.

FIG. 5. Distribution of the transverse energy of all b jets in events with a superjet and in the complementary sample.
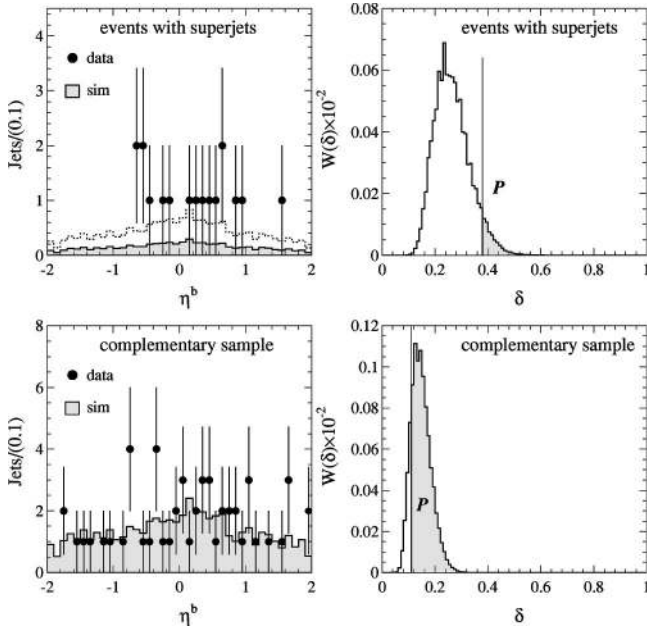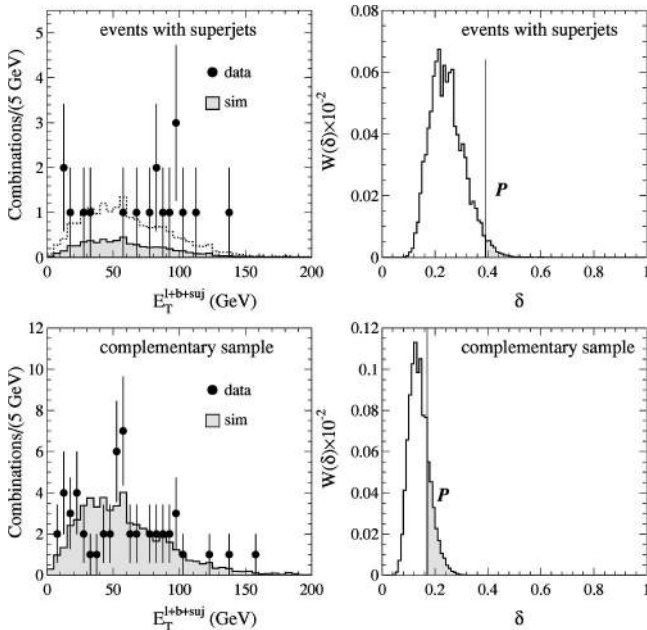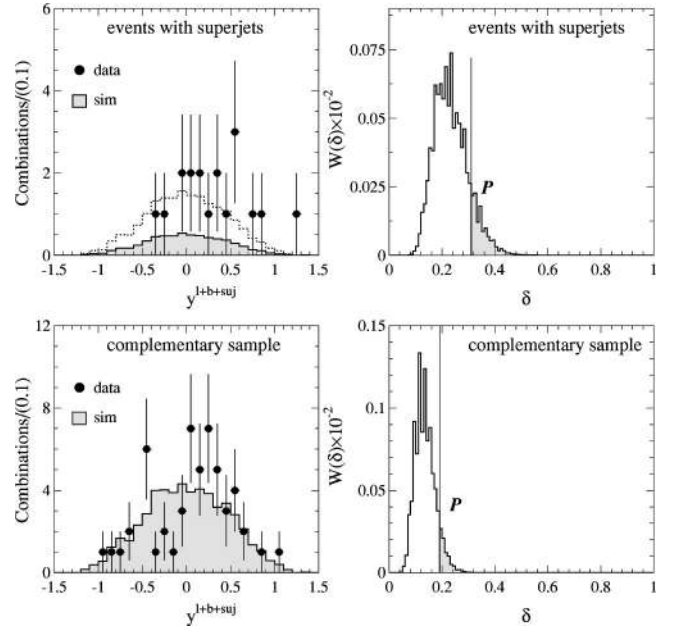
FIG. 6. Distribution of the pseudorapidity of all *b* jets in events with a superjet and in the complementary sample.

simulation is much reduced for this second set of variables. The probability distribution of the KS comparisons for the 18 kinematic distributions is shown in Fig. 11.

As indicated by the figure, the probabilities of the complementary sample appear to be flatly distributed, as expected for a set of distributions consistent with the simulation. In contrast, the probabilities of the superjet events cluster at low values. This indicates the difficulty of our simulation to de-

FIG. 8. Distribution of the rapidity of the system *l* + superjet + *b*-jet in events with a superjet and in the complementary sample.

scribe the kinematics of events with a superjet. Given the *a posteriori* selection of the nine kinematic variables, the combined statistical significance of the observed discrepancies cannot be unequivocally quantified. A thorough discussion of this issue is beyond the goal of this paper, which is meant to present the basic measurements. We leave additional studies of these events and their possible interpretation to other publications. The characteristics of these events are listed in Ap-
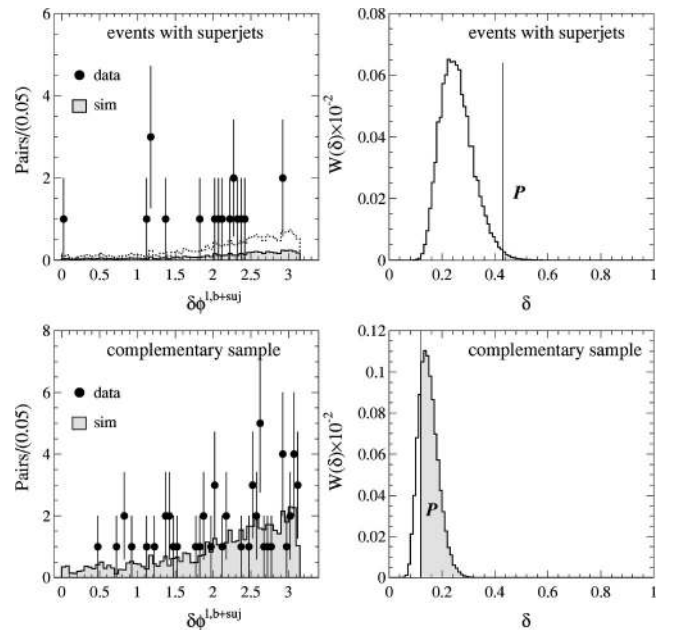

FIG. 7. Distribution of the transverse energy of the system *l* + superjet + *b*-jet in events with a superjet and in the complementary sample.

FIG. 9. Distribution of the azimuthal angle between the primary lepton and the superjet + *b*-jet system in events with a superjet and in the complementary sample.

TABLE VII. Results of the KS comparison between data and simulation. For each variable we list the observed KS distance δ^0 and the probability P of making an observation with a distance no smaller than δ^0.

Variable	Events with a superjet		Complementary sample	
	δ^0	P (%)	δ^0	P (%)
E_T^l	0.47	2.6	0.14	70.9
η^l	0.54	0.10	0.12	72.7
E_T^{suj}	0.38	11.1	0.15	43.0
η^{suj}	0.36	15.2	0.13	73.4
E_T^b	0.36	6.7	0.18	8.6
η^b	0.38	6.8	0.11	80.0
$E_T^{l+b+suj}$	0.39	2.5	0.17	18.8
$y^{l+b+suj}$	0.31	13.8	0.19	7.8
$\delta\phi^{l,b+suj}$	0.43	1.0	0.12	77.9
Z_{vrtx}	0.48	1.7	0.16	50.5

pendix B.

VIII. CHECK OF THE ISOLATION AND LIFETIME OF THE PRIMARY AND SOFT LEPTONS

The kinematics of the primary leptons in events with a superjet is poorly described by the SM simulation, in which they are mostly contributed from W decays. Therefore, we cross-check that the excess of events with a superjet is not due to a misestimate of the number of non-W events. According to the SM prediction, the small background of tagged non-W events is due to semileptonic decays in $b\bar{b}$ and $c\bar{c}$ events. In such a case, the primary leptons are not isolated and have large impact parameters because of the long b and c quark lifetime. Figure 12 shows that primary leptons in the 13 events with a superjet are at least as well isolated as primary leptons in the complementary sample. Distributions of the signed impact parameter significance of the primary lepton track are also shown in Fig. 12. Tracks from long-lived decays usually have large (≥ 3) impact parameter significance. The primary leptons in the 13 events are consistent with being prompt. One also notes that in the complementary sample two events have a primary lepton with large positive impact parameter; this is consistent with our estimate of

2.10$\pm$0.05 non-W events (mostly from b decays).

Based on the SM expectation, the average transverse momenta of primary and soft leptons are expected to differ by an order of magnitude (they are selected with a 20 and 2 GeV/c transverse momentum requirement, respectively). However, in the data the average transverse momenta are 35 and 13 GeV/c, respectively. Since the $W+\geq 1$ jet sample has been selected by removing all events containing a second lepton candidate with isolation $I \leq 0.15$ and transverse momentum $p_T \geq 10$ GeV/c, the superjets could be due to dilepton events which are not removed because the second lepton happens to be merged with a jet and is not isolated. We have removed only 16 dilepton candidate events tagged by SECVTX from the $W+2,3$ jet sample. From the simulation we expect that less than 0.5 events will have the second lepton randomly distributed in a cone of radius 0.4 around the axis of the jet tagged by SECVTX. Figure 13 shows that soft leptons are mostly found close to the superjet axis and are not uniformly distributed over the jet clustering cone of radius $R=0.4$. We have also looked at the distribution of the signed impact parameter significance of SLT tracks. Figure 13 shows that, in contrast with primary leptons, soft leptons inside a superjet are not prompt. As expected from the simu-

TABLE VIII. KS comparison of additional kinematical variables. For each variable we list the observed KS distance δ^0 and the probability P of making an observation with a distance no smaller than δ^0.

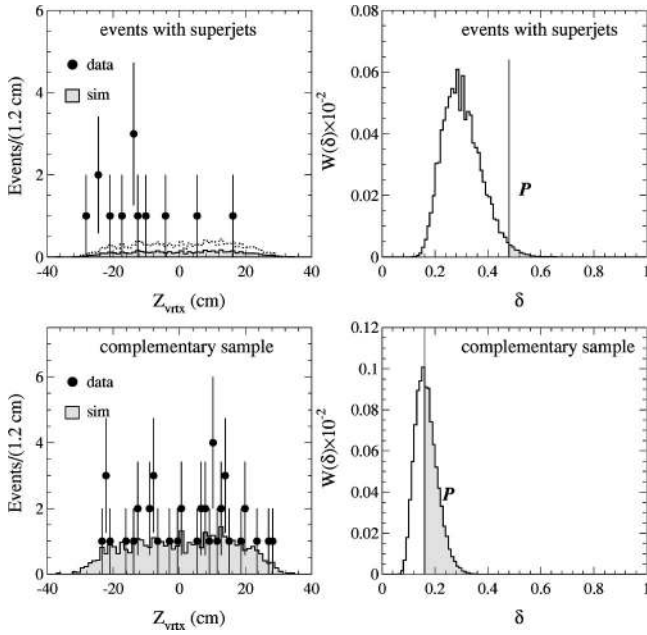| Variable	Events with a superjet		Complementary sample	
	δ^0	P (%)	δ^0	P (%)
$\not{E}_T$	0.31	27.1	0.14	57.1
M_T^W	0.36	13.1	0.16	38.2
M^{b+suj}	0.36	4.0	0.12	58.9
y^{b+suj}	0.35	7.1	0.14	34.9
E_T^{b+suj}	0.28	24.0	0.10	60.1
$M^{l+b+suj}$	0.31	21.0	0.15	33.6
$\delta\theta^{b,suj}$	0.26	30.1	0.15	41.1
$\delta\phi^{b,suj}$	0.31	15.3	0.10	83.8
$\delta\theta^{l,b+suj}$	0.25	37.3	0.16	35.7

FIG. 10. Distribution of the event-vertex position along the beam line (z axis) in events with a superjet and in the complementary sample.

lation of heavy flavor decays, the soft lepton track is part of the SECVTX tag in 8 out of 13 superjets.

IX. ADDITIONAL PROPERTIES OF THE SUPERJETS

In this section we compare other properties of the superjets to the W+jet simulation to verify if, independent of the excess of soft lepton tags and the discrepancies found in Sec. VII, they are otherwise compatible with being produced by semileptonic decays of b and c hadrons.

A. Lifetime

A measure of the lifetime of the hadron producing a secondary vertex is
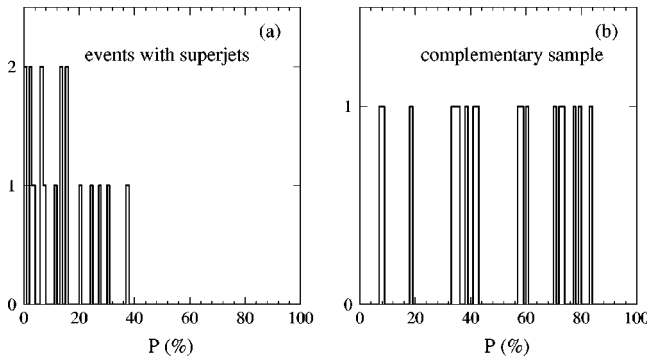
FIG. 11. Distribution of the probabilities P that the 13 events with a superjet (a) and the complementary sample (b) are consistent with the SM prediction. The distribution (a) has a mean of 0.13 and a RMS of 0.11; the distribution (b) has a mean of 0.50 and a RMS of 0.24.
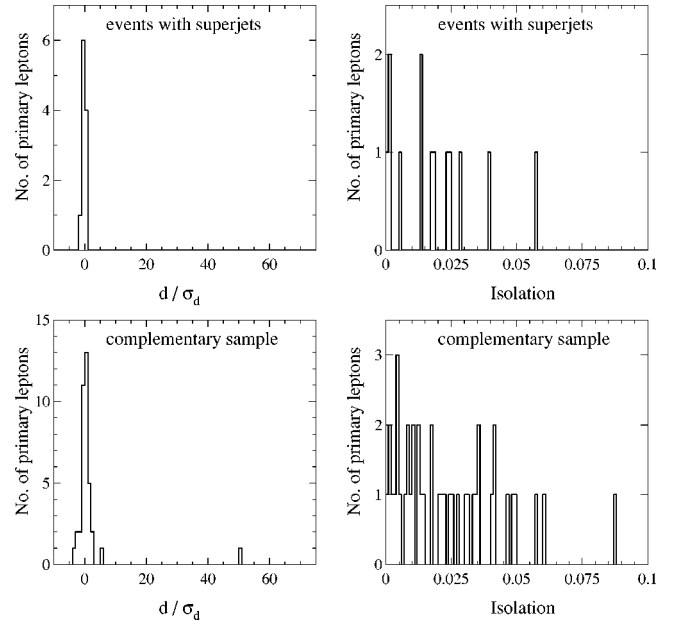

FIG. 12. Distributions of the signed impact parameter significance (d/σ_d) and of the isolation of primary leptons.

$$\text{pseudo-}\tau = \frac{L_{xy}}{c} \frac{M^{SVX}}{p_T^{SVX}},$$

where L_{xy} is the projection of the transverse displacement of the secondary vertex on the jet axis, M^{SVX} is the invariant mass and p_T^{SVX} is the total transverse momentum of all tracks associated with the secondary vertex. In this measurement, the Lorentz boost of the heavy flavor hadron is approximated with the Lorentz boost of the SECVTX tag.

Pseudo-τ distributions are compared in Fig. 14 to the simulation based on the sample compositions for the superjet and complementary sample. The number of simulated superjets is rescaled to 13 events. One notes that data and simulation have quite similar pseudo-τ distributions. The pseudo-τ calculation does not account for the neutral particles emitted in the heavy flavor decay. As a result a kinematic correction factor is needed to convert it into a lifetime measurement. In the case of beauty or charmed mesons, this factor is approximately 1.1.
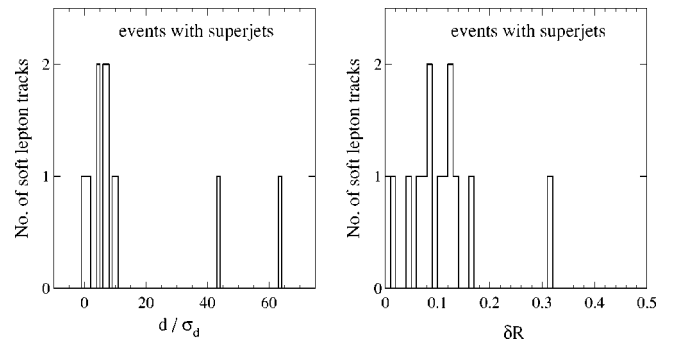

FIG. 13. Distributions of the signed impact parameter significance of soft lepton tracks and of their distance $\delta R = \sqrt{\delta\phi^2 + \delta\eta^2}$ from the superjet axis.
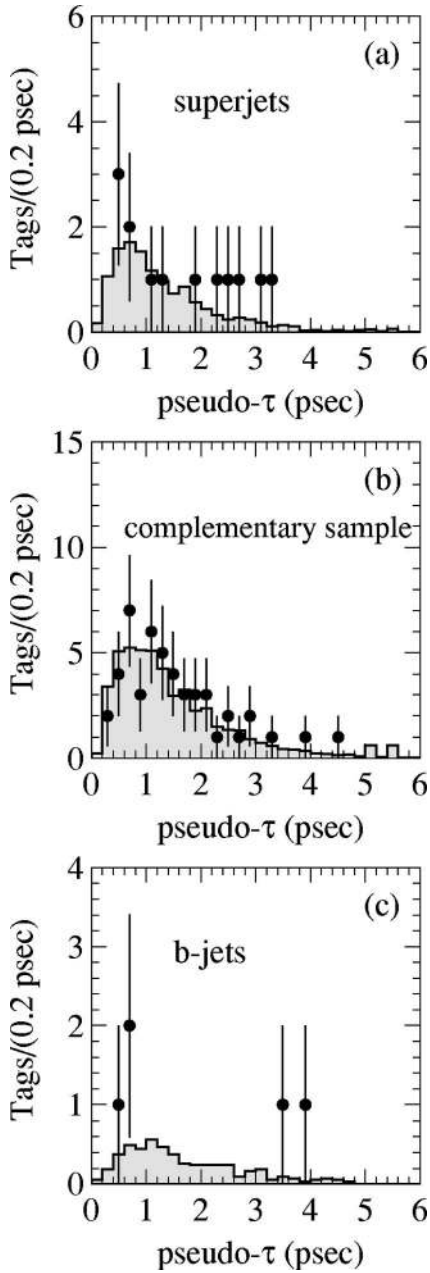
FIG. 14. Pseudo-τ distributions for superjets (a) and for tagged jets in the complementary sample (b) are compared to the simulation (shaded histograms). The distribution for additional SECVTX tagged jets in superjet events (c) is compared to simulated b jets.

A measure of the lifetime independent of the Lorentz boost is provided by $\tau_{ip} = (4/\pi)(\langle d_0 \rangle / c)$, where $\langle d_0 \rangle$ is the error-weighted average impact parameter of all tracks that form a SECVTX tag and have positive signed impact parameter. The distribution of the ratio $R_\tau = \tau_{ip}/\text{pseudo-}\tau$ provides a check of the kinematic correction factor.

We first show that our simulation correctly models the correlation between the lifetime measured with pseudo-τ and τ_{ip} by using the generic-jet samples described in Appendix A. Figures 15 and 16 show that both methods yield consistent lifetime measurements in the data and in the simulation in which SECVTX tags are produced by b and c hadrons. In
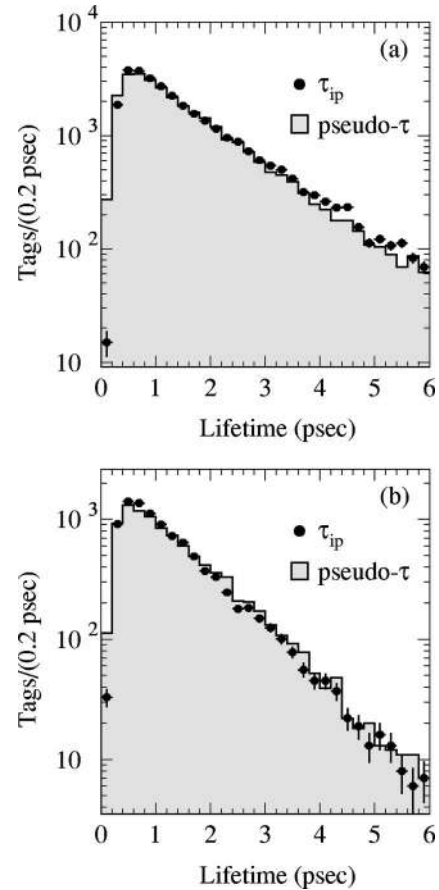

FIG. 15. Comparison of lifetime distributions using the pseudo-τ and τ_{ip} method in generic-jet data (a) and in the corresponding simulation (b).

this comparison, the contribution of fake tags in jets without heavy flavor is removed by subtracting the observed distribution of negative SECVTX tags (see Sec. IV A).

Figure 17 presents the R_τ distributions in superjet events and in the complementary sample. The result of the usual KS comparisons (see Sec. VII C) between the data and the simulation are listed in Table IX and indicate overall agreement. As shown in Fig. 18, the distributions of the invariant mass M^{SVX} are also correctly modeled by the simulation. The transverse momentum distribution of SECVTX tags is discussed in Sec. IX B.

B. Transverse momentum distribution of SLT tags

Figure 19 compares the distribution of p_T^{SLT}, the soft lepton transverse momentum, in the 13 superjets to the simulation based on the sample composition listed in Table V. The p_T^{SLT} spectrum depends on the jet transverse energy, and the superjet transverse energy distribution in the data is stiffer than in the SM expectation (see Fig. 3). Therefore, we have corrected the transverse energy distribution of simulated superjets to make it look like the data. Figure 19 shows that soft leptons in superjet events have transverse momenta larger than what is expected for semileptonic decays of b and c quarks. By construction the complementary sample does
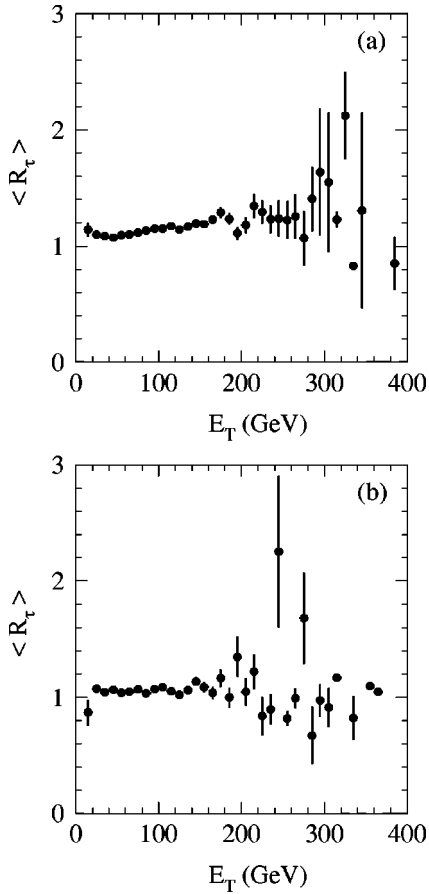
FIG. 16. Yield of $\langle R_\tau \rangle = \langle (\text{pseudo} - \tau)/\tau_{ip} \rangle$ as a function of the jet transverse energy in generic-jet data (a) and in the corresponding simulation (b).

not contain soft lepton tags. However, p_T^{SVX}, the total transverse momentum of all tracks forming a SECVTX tag, is a useful analogue. If the difference between the transverse momentum of the soft lepton tag in the data and the simulation were due to inadequate modeling of the hadronization process, the p_T^{SVX} distribution in the complementary sample would also disagree with the simulation. However, Figure 20a shows agreement between the complementary sample and the simulation.[6] The result of the KS comparison of these distributions is also listed in Table IX. The probability that the p_T^{SVX} distribution in the complementary sample is produced according to the simulation is $P=47\%$. The probability that the p_T^{SLT} distribution in superjets is consistent with the SM simulation is $P=0.1\%$.

C. Comparison of p_T^{SLT} and p_T^{SVX} distributions in generic-jet data to the simulation

We compare superjets in generic-jet data and in the corresponding simulation to check if the discrepancy between the observed and predicted transverse momentum distribu-

---

[6]Since most of the SLT tracks are associated with the secondary vertex, the p_T^{SVX} distribution for superjets appears stiffer than in the complementary sample and in the simulation.
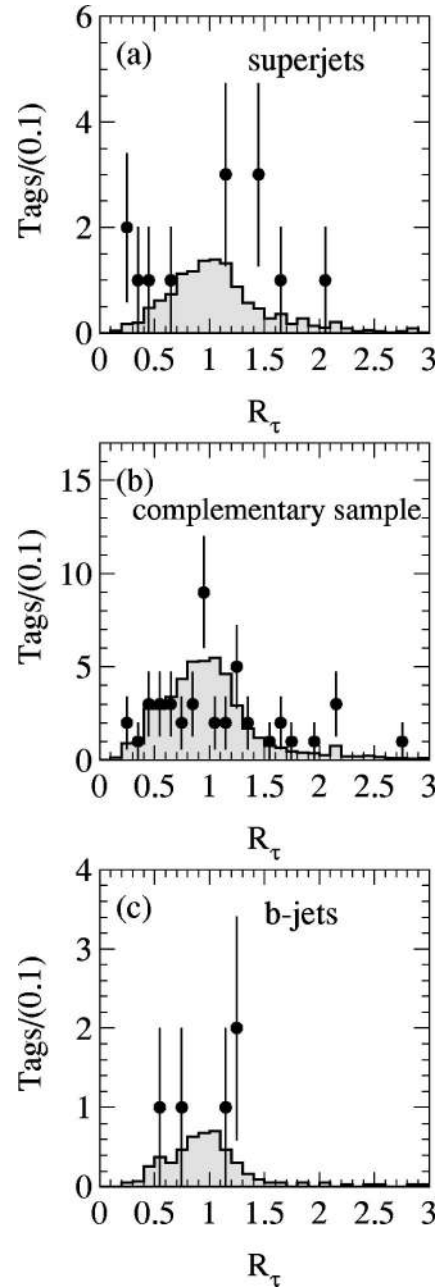

FIG. 17. Distributions of the variable R_τ (see text) for superjets (a) and for tagged jets in the complementary sample (b) are compared to the simulation (shaded histograms). The distribution for b jets in superjet events (c) is compared to simulated b jets.

tion of soft lepton tags is due to the modeling of semileptonic decays in QQ or to the modeling of the hadronization in HERWIG. The generic-jet data and simulation are described in Appendix A. The heavy flavor content of this sample is similar to that of $W+2,3$ jet events. We normalize data and simulation to the same number of events and in both we search for jets which contain positive and negative SECVTX tags. We then search for additional soft lepton tags in jets tagged by SECVTX. The data and simulation contain approximately the same number of supertags as a result of the calibration of the SLT efficiency in the simulation (see Appendix A). Fake SECVTX tags are evaluated and removed using the number

TABLE IX. Result of KS comparisons between data and simulation. For each variable we list the observed KS distance δ^0 and the probability P of making an observation with a distance no smaller than δ^0.

Variable	Events with a superjet δ^0	P (%)	Complementary sample δ^0	P (%)
R_τ (superjets)	0.44	4.7	0.15	35.1
R_τ (b jets)	0.44	39.0		
M^{SVX}	0.20	56.9	0.10	51.4
p_T^{SLT}	0.55	0.09		
p_T^{SVX}			0.14	47.4

of observed negative SECVTX tags in the data and the simulation. We do not remove the contribution of fake SLT tags from the data but we add fake SLT tags to the simulation by weighting each track in a simulated jet with the same SLT fake probability normally used to evaluate the rate of fake tags in the data.

In 5.5×10^5 generic-jet events we find 1324 events with a supertag in the data and 1342 in the simulation. Distributions of the transverse momentum of soft lepton tags and of all tracks forming a SECVTX tag are shown in Fig. 21. The agreement between data and simulation provides evidence that we correctly model b and c jets.

X. ADDITIONAL CROSS-CHECKS

The selection criteria used in this analysis were optimized for finding the top quark [4]. The high-p_T inclusive lepton data set, from which we have selected the sample used in this study, consists of about 82 000 events with one or more jets before making requirements on the transverse momentum and isolation of the primary lepton and on the missing transverse energy. Half of these events have primary leptons which are not well isolated ($I \geqslant 0.2$). They are mostly due to multijet production with one jet containing a fake lepton, but also include a small amount of $b\bar{b}$ and $c\bar{c}$ production. The $p_T \geqslant 20$ GeV/c, $I \leqslant 0.1$, and $\not{E}_T \geqslant 20$ GeV cuts reduce this data set to an almost pure W+jet sample of about 11 000 events. In Sec. X A we investigate the rate of superjets in the

FIG. 19. The distribution of the transverse momentum of soft leptons in superjet events is compared to the SM expectation normalized to the same number of tags and corrected for the superjet E_T distribution. One superjet contains two soft leptons.

kinematic regions removed in the original selection of the $W+\geqslant 1$ jet sample. This checks that events with a superjet are not the tail of a large unexpected background. In Sec. X B we look at the effect of removing the trigger requirement for primary muons and in Sec. X C we extend our search to

FIG. 20. Distributions of the transverse momentum of all tracks forming a SECVTX tag in the complementary sample (a) and in superjets (b).
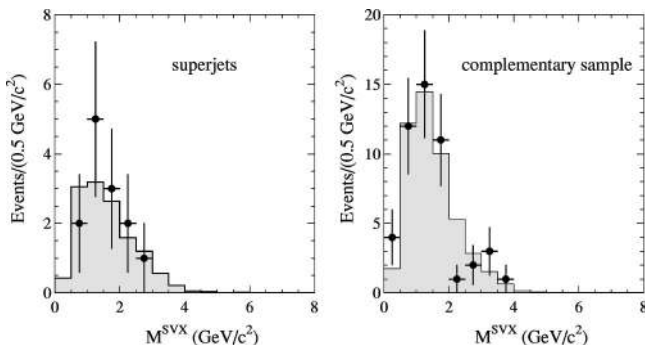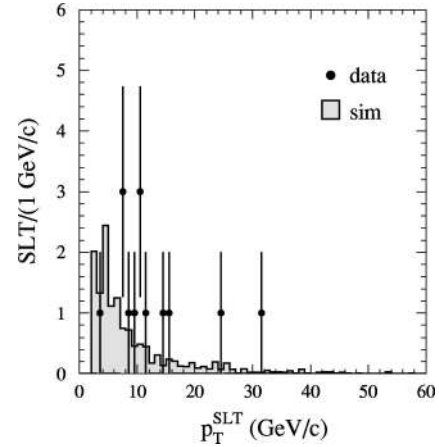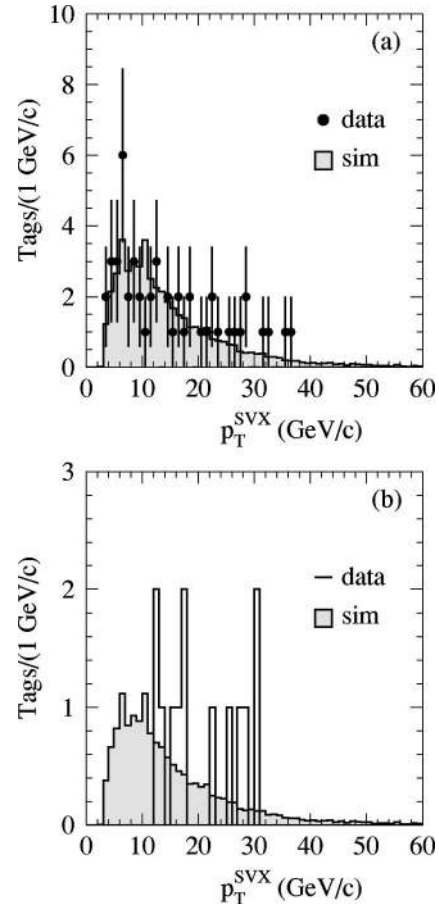

FIG. 18. Distributions of M^{SVX}, the invariant mass of the tracks associated with a secondary vertex, are compared to the simulation (shaded histograms) normalized to the same number of events.
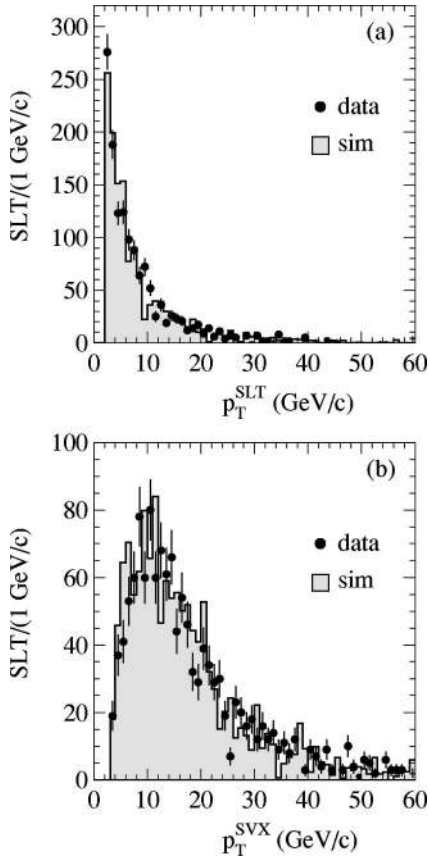
FIG. 21. Distributions of the transverse momentum of soft leptons (a) and of all tracks forming the SECVTX tags (b) in superjets selected in generic-jet data and in the corresponding SM simulation. Data and simulation are normalized to the same number of events before tagging.

events with a primary electron in the plug calorimeter.

A. Dependence on $\not{E}_T$ and on the isolation and transverse momentum of the primary lepton

There are 36 677 events with a primary lepton with $p_T \geq 20$ GeV/c and $I \leq 0.2$; 615 events have SECVTX tags (their I vs $\not{E}_T$ distribution is shown in Fig. 22). Using nominal cuts for selecting the primary lepton, we first study the rate of supertags in events tagged by SECVTX when $\not{E}_T \leq 20$ GeV. With the exception of non-W events, which are the largest fraction, the relative contribution of all other SM processes does not depend on $\not{E}_T$. Since the ratios of supertags to SECVTX tags in non-W events and in the sum of the remaining processes are quite similar, in this case we predict the number of supertags in this sample by multiplying the number of observed SECVTX tags by the predicted ratio of supertags to SECVTX tags for events with $\not{E}_T \geq 20$ GeV. The observed number agrees with the expectation as shown in Table X.

In Table XI we compare rates of supertags in events tagged by SECVTX when the isolation of the primary lepton is large. These events are mostly contributed by $b\bar{b}$ production. The number of observed supertags in events with $\not{E}_T$
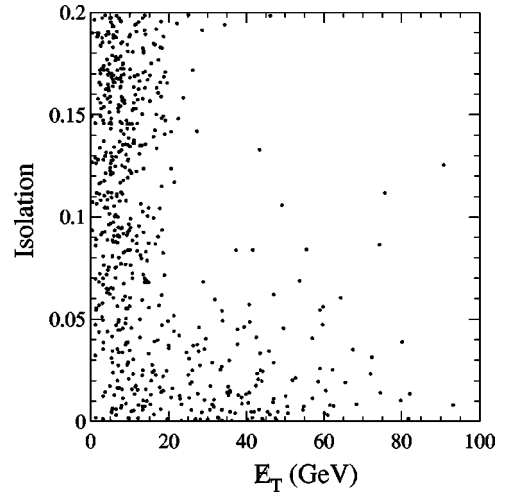

FIG. 22. Distribution of primary lepton isolation vs $\not{E}_T$ for events containing one or more jets tagged by SECVTX. The primary lepton transverse momentum is larger than 20 GeV/c.

≥ 20 GeV is consistent with the prediction of the method used to estimate the non-W background (we multiply the number of SECVTX tags in events with $\not{E}_T \geq 20$ GeV by the ratio of supertags to SECVTX tags in events with $\not{E}_T \leq 20$ GeV).

As shown in Fig. 1, many primary leptons in superjet events have transverse momentum close to the threshold used to select the sample. We have checked that we are not observing the tail of a distribution peaking at small transverse momenta by first removing the 20 GeV/c transverse momentum cut on the primary lepton (the p_T threshold of the L3 trigger is about 18 GeV/c). Before tagging the size of the $W+$ jet sample increases by 20%. As shown in Table XII, no additional events with a supertag are found.

We then have searched for events with a superjet in the low-p_T inclusive lepton sample collected during the 1994–1995 collider run (run 1B) using a L3 trigger threshold of 8 GeV/c (8 of the 13 events with a superjet were collected in run 1B). Because of the lower threshold, the trigger rate was prescaled by a factor of 1.3. In this sample we find seven events having a primary lepton with $p_T \geq 10$ GeV/c and $I \leq 0.1$, $\not{E}_T \geq 20$ GeV, and containing a superjet and one or two additional jets. Six of the seven events are the same events found in the high-p_T inclusive lepton sample; the additional event contains a primary electron with $E_T = 17.7$ GeV.

TABLE X. Number of tagged events as function of the jet multiplicity. The events are selected by requiring $\not{E}_T \leq 20$ GeV and a primary lepton with $p_T \geq 20$ GeV/c and $I \leq 0.1$. The predicted number of supertags is based upon the observed number of SECVTX tags (see text).

Tag type	1 jet	2 jets	3 jets	≥ 4 jets
SECVTX	168	21	7	6
Supertag	12	1	0	0
Prediction	10.2 ± 1.3	1.2 ± 0.2	0.5 ± 0.2	0.5 ± 0.2

TABLE XI. Yield of events with supertags as function of the jet multiplicity. We select primary leptons with $p_T \geq 20$ GeV/c and isolation $0.1 \leq I \leq 0.2$. The prediction of supertags in events with $\not{E}_T \geq 20$ GeV is derived using the ratio of supertags to SECVTX tags in events with $\not{E}_T \leq 20$ GeV.

Tag type	1 jet	2 jets	3 jets	$\geq$4 jets
		$\not{E}_T \leq 20$ GeV		
SECVTX	220	33	10	2
Supertag	17	4	2	1
		$\not{E}_T \geq 20$ GeV		
SECVTX	8	3	5	0
Supertag	2	0	1	0
Prediction	0.6 ± 0.1	0.4 ± 0.2	1.0 ± 0.7	0

B. Removal of the trigger requirement for primary muons

In selecting the events used in this analysis, we require that the primary lepton has fired the appropriate second level (L2) trigger (see Sec. III A). The second level of the muon trigger requires a match between a CTC track reconstructed by a fast track processor [34] and a track segment in the muon chambers, which fired the first level trigger [4,7]. The L2 trigger efficiency for primary muons is approximately 70% [7]. Based on the observed 13 events with a superjet, we should have lost about two such events because the primary muon failed the muon trigger (the detector has about the same acceptance for electrons and muons). However, the original high-p_T lepton data set contains also events triggered by other objects in the events. As shown in Fig. 19, 85% of the superjets contain a soft lepton with transverse momentum comparable or larger than the L2 trigger threshold. If the observed transverse momentum distribution of the soft leptons is not a statistical fluctuation, we could find in the original data sample one or two additional events with a supertag in which the primary muon failed the trigger but the event was rescued by the soft muon. On the other hand, according to the SM simulation, only 9.6% of the W+jet events with a SLT tag contain a soft muon which passes the trigger p_T requirement. Using the predicted rates listed in Table III, we estimate that 31 W+1 jet events and 12 W+2,3 jet events with a primary muon have failed the trigger; three W+1 jet events and 1.1 W+2,3 jet events can be rescued by a soft muon. Of these events, 0.09 W+1 jet and 0.08 W+2,3 jet events are expected to contain a jet with a supertag.

In the data, after removing the trigger requirement on the primary muon, we recover three W+1 jet events, none of which contains supertags. We also recover one W+2 jet and

TABLE XII. Numbers of tagged W+jet events with $\not{E}_T \geq 20$ GeV and primary leptons with $I \leq 0.1$ and $p_T \leq 20$ GeV/c.

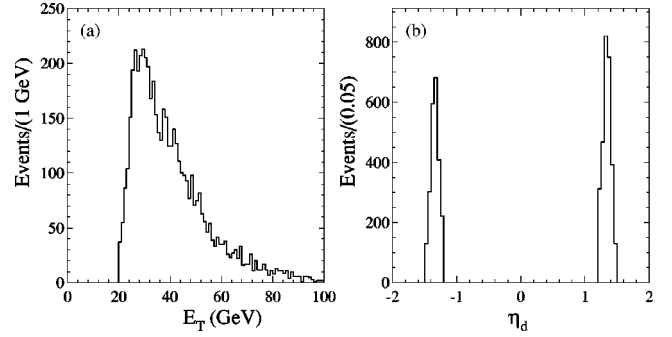| Tag type	W+1 jet	W+2 jet	W+3 jet	$W+\geq$4 jet
SECVTX	2	0	0	1
Supertag	0	0	0	0

FIG. 23. Distributions of the transverse momentum and the pseudorapidity with respect to the nominal interaction point of plug electrons.

one W+3 jet event, both with a supertag. No extra W+4 jet event is found. The characteristics of these two events are listed in Appendix B.

C. Study of plug electrons

As shown in Fig. 2, the pseudorapidity distribution of primary leptons in events with a superjet appears to rise at the end of the central detector acceptance ($|\eta| \simeq 1$). Motivated by this observation, we have searched for events with a superjet using primary electrons in the plug calorimeter. The pseudorapidity and transverse momentum distributions of plug electrons are shown in Fig. 23. We select W+jet events requiring an isolated plug electron with $E_T \geq 20$ GeV and $\not{E}_T \geq 20$ GeV.

Table XIII lists rates of W+jet events with a primary plug electron before and after tagging. We observe two additional W+2,3 jet events with a supertag, when 0.34 ± 0.04 events are expected from known processes. The characteristics of these two additional events with a superjet are listed in Appendix B.

XI. CONCLUSIONS

We have carried out a study of the heavy flavor content of jets produced in association with W bosons. Comparisons of the observed rates of SECVTX (displaced vertex) and SLT (soft lepton) tags with standard model predictions, including NLO calculations of single and pair produced top quarks, are generally in good agreement. However, we find an excess of events which have jets with both SECVTX and SLT heavy flavor tags. The standard model expectation for these W+2,3 jet events is 4.4 ± 0.6 events, while 13 are observed. A detailed examination of the kinematic properties of these events finds that they are statistically difficult to reconcile with a simulation of standard model processes, which well reproduces closely related samples of data. Although obscure detector effects can never be ruled out, extensive studies of these events and investigations of larger statistics samples of generic-jet data have not revealed any effects which indicate the existence of detector problems or simulation deficiencies. We are not aware of any model for new physics which incorporates the production and decay properties necessary to explain all features of these events. Work is continuing on

TABLE XIII. Number of events with an isolated plug electron and $\not{E}_T \geqslant 20$ GeV before and after tagging. Since the relative contributions of different processes are not affected by the difference in the pseudorapidity range covered by central leptons and plug electrons, the prediction of supertags is derived from Table V after normalizing to the same number of SECVTX tags.

Source	$W + 1$ jet	$W + 2$ jet	$W + 3$ jet	$W + \geqslant 4$ jet
Data	1245	243	52	11
SECVTX tags	15	3	1	1
Supertags	3	2	0	0
SM prediction	0.9 ± 0.1	0.24 ± 0.03	0.10 ± 0.02	0.10 ± 0.03

studies of the present data. With much larger data samples from the Run II of the Tevatron, we will be able to explore in greater detail this class of events.

APPENDIX A: COMPARISON OF RATES OF SUPERTAGS IN GENERIC-JET DATA AND IN THE CORRESPONDING SIMULATION

Table XIV lists rates of tags in generic-jet data and in the corresponding simulation. This comparison profits from the measurement of the heavy flavor composition of generic-jet data and of the calibration of the HERWIG generator presented in Ref. [7]. A summary of that study is provided here. Generic-jet data are events collected by requiring at least one jet with transverse energy above trigger threshold (i.e., a 20 GeV threshold for JET 20 data). As usual we consider jets with $E_T \geqslant 15$ GeV and pseudorapidity $|\eta| \leqslant 2$. We apply the additional requirement that at least one of the jets in the event contains two SVX tracks and is therefore taggable by SECVTX or JPB. An equal number of $2 \rightarrow 2$ hard-scattering events is simulated using option 1500 of the HERWIG generator and the MRS (G) parton distribution functions [35]. In the simulation, jets with heavy flavor come from heavy quarks in the initial or final state of the hard scattering (flavor excitation and direct production) or from gluon splitting. A 13.2% fraction of the simulated jets contains heavy flavor (4.7% due to b hadrons and 8.5% due to c hadrons). A 3.5% fraction of the simulated jets contains heavy flavor and is

TABLE XIV. Number of tags due to heavy flavors observed in generic-jet data and in the simulation normalized to the same number of events before tagging. The number of mistags removed from the data is indicated in parentheses; errors include a 10% uncertainty in the mistag evaluation. The error of the number of simulated SLT tags includes the 10% uncertainty on the SLT tagging efficiency. This error is not included for simulated SECVTX + SLT and JPB + SLT tags as we intend to calibrate the simulation efficiency with the data.

Tag type	Data (removed fakes)	Simulation
JET 20 (194 009 events)		
SECVTX	4058 ± 92 (616.0)	4052 ± 143
JPB	5542 ± 295 (2801.0)	5573 ± 173
SLT	1032 ± 402 (3962.0)	826 ± 122
SLT + SECVTX	219.8 ± 20 (94.2)	263 ± 29
SLT + JPB	287.3 ± 28 (166.7)	330 ± 29
JET 50 (151 270 events)		
SECVTX	5176 ± 158 (1360.0)	5314 ± 142
JPB	6833 ± 482 (4700.0)	6740 ± 171
SLT	1167 ± 530 (5241.0)	1116 ± 111
SLT + SECVTX	347 ± 29 (169.0)	404 ± 22
SLT + JPB	427.5 ± 42 (288.5)	490 ± 32
JET 100 (129 434 events)		
SECVTX	5455 ± 239 (2227.0)	5889 ± 176
JPB	6871 ± 659 (6494.0)	7263 ± 202
SLT	1116 ± 642 (6367.0)	1160 ± 168
SLT + SECVTX	377.6 ± 36 (243.4)	508 ± 35
SLT + JPB	451.8 ± 55 (401.2)	563 ± 34

TABLE XV. Fractions of SECVTX and JPB tags with a supertag in generic-jet data and in the corresponding simulation. In the simulation the fraction of supertags is slightly higher than in the data, independent of the jet transverse energy and the heavy flavor type.

| | JET 20 | | JET 50 | | JET 100 | |
	$\dfrac{\text{SLT}+\text{SECVTX}}{\text{SECVTX}}$	$\dfrac{\text{SLT}+\text{JPB}}{\text{JPB}}$	$\dfrac{\text{SLT}+\text{SECVTX}}{\text{SECVTX}}$	$\dfrac{\text{SLT}+\text{JPB}}{\text{JPB}}$	$\dfrac{\text{SLT}+\text{SECVTX}}{\text{SECVTX}}$	$\dfrac{\text{SLT}+\text{JPB}}{\text{JPB}}$
Data	0.054 ± 0.005	0.052 ± 0.006	0.067 ± 0.006	0.063 ± 0.008	0.069 ± 0.007	0.066 ± 0.010
Simulation	0.065 ± 0.007	0.059 ± 0.005	0.076 ± 0.004	0.073 ± 0.005	0.086 ± 0.006	0.077 ± 0.005
Data/Simulation	0.83 ± 0.12	0.88 ± 0.13	0.88 ± 0.09	0.86 ± 0.12	0.80 ± 0.10	0.86 ± 0.14

tagged by SECVTX (73% of the tagged jets are initiated by a b quark and 27% by a c quark). Jet probability is more efficient than SECVTX in tagging c jets. A 4.6% fraction of the simulated jets contains heavy flavor and is tagged by jet probability (55% of the tagged jets are initiated by a b quark and 45% by a c quark).

The heavy flavor production cross sections calculated by HERWIG have been tuned in Ref. [7] to reproduce the pattern of SECVTX and JPB tags observed in generic-jet data.

HERWIG gives a good description of the data provided that the direct and flavor excitation production cross sections are increased by 1.10 ± 0.16 and the fraction of gluons branching to heavy quarks is increased by 1.36 ± 0.22. The accuracy of this calibration is limited by our understanding of the tagging efficiencies. The factors required to calibrate simulated rates of SECVTX or JPB tags are determined more accurately: 1.1 ± 0.1 for direct and flavor excitation production and 1.38 ± 0.09 for gluon splitting.

TABLE XVI. Characteristics of $W+2$ jet events with a superjet. Jets tagged by the SECVTX (SLT) algorithm are labeled SECVTX (SLT). Jet energies are corrected for calorimeter nonlinearities and out-of-cone losses; $\not{E}_T$ is evaluated after these corrections are applied.

	p_T (GeV/c)	η	ϕ (rad)		p_T (GeV/c)	η	ϕ (rad)
Run 46 935 event 266 805				Run 41 540 event 127 085			
electron $(-)$	29.7	-0.87	0.15	electron $(-)$	22.2	0.84	0.57
Jet 1	49.6	-0.61	5.46	Jet 1 (SECVTX,SLT)	144.5	0.11	6.15
Jet 2 (SECVTX,SLT)	41.1	0.43	2.70	Jet 2	61.5	-0.54	3.75
$\not{E}_T$	19.8		2.56	$\not{E}_T$	92.1		3.05
SLT (μ^-)	3.8	0.52	2.63	SLT (μ^+)	8.8	0.18	6.14
Z_{vrtx} (cm)	-20.71			Z_{vrtx} (cm)	-4.77		
Run 41 627 event 87 219				Run 61 167 event 368 226			
electron $(-)$	78.5	0.90	4.56	electron $(+)$	22.2	0.76	1.37
Jet 1	68.7	0.11	3.03	Jet 1 (SECVTX,SLT)	99.3	-0.16	1.86
Jet 2 (SECVTX,SLT)	58.0	0.50	1.23	Jet 2 (SECVTX)	68.1	0.93	5.48
$\not{E}_T$	47.4		0.23	$\not{E}_T$	36.0		3.61
SLT (μ^-)	10.4	0.47	1.26	SLT (μ^-)	24.7	-0.11	1.92
Z_{vrtx} (cm)	-28.11			Z_{vrtx} (cm)	-14.20		
Run 65 384 event 266 051				Run 65 741 event 654 870			
electron $(-)$	21.9	0.68	0.65	muon $(+)$	47.2	0.79	6.01
Jet 1	73.9	2.06	0.33	Jet 1 (SECVTX,SLT)	109.4	0.63	4.58
Jet 2 (SECVTX,SLT)	59.0	0.61	4.92	Jet 2 (SECVTX)	63.9	0.31	2.87
$\not{E}_T$	96.2		3.02	$\not{E}_T$	95.8		1.31
SLT (μ^+)	10.9	0.61	4.80	SLT (e^+)	7.1	0.76	4.61
Z_{vrtx} (cm)	-24.24			Z_{vrtx} (cm)	-14.20		
Run 46 357 event 511 399				Run 69 520 event 136 405			
muon $(-)$	22.2	-0.82	5.64	electron $(-)$	20.4	1.01	0.25
Jet 1	58.2	-0.20	6.10	Jet 1	44.2	-0.61	5.57
Jet 2 (SECVTX,SLT)	41.2	0.27	2.84	Jet 2 (SECVTX,SLT)	32.7	-0.88	2.71
$\not{E}_T$	39.8		2.89	$\not{E}_T$	27.5		2.42
SLT (μ^+)	15.2	0.25	2.96	SLT (μ^+)	11.3	-0.87	2.71
SLT (e^-)	7.1	0.38	2.89	Z_{vrtx} (cm)	-12.36		
Z_{vrtx} (cm)	-24.13						

TABLE XVII. Characteristics of $W+3$ jet events with a superjet. Jets tagged by the SECVTX (SLT) algorithm are labeled SECVTX (SLT). Jet energies are corrected for calorimeter nonlinearities and out-of-cone losses; $E\!\!\!/_T$ is evaluated after these corrections are applied.

	p_T (GeV/c)	η	ϕ (rad)		p_T (GeV/c)	η	ϕ (rad)
Run 56 911 event 114 159				Run 61 548 event 284 898			
electron $(-)$	58.5	0.92	0.83	muon $(+)$	20.3	−0.54	3.00
Jet 1	203.4	−0.13	2.93	Jet 1	72.4	0.55	1.96
Jet 2 (SECVTX,SLT)	65.5	0.82	5.80	Jet 2 (SECVTX)	64.9	0.44	3.94
Jet 3	24.1	0.60	0.00	Jet 3 (SECVTX,SLT)	58.7	0.07	5.73
$E\!\!\!/_T$	61.5		5.41	$E\!\!\!/_T$	38.8		0.02
SLT (μ^+)	9.3	0.77	5.75	SLT (e^-)	14.6	0.09	5.83
Z_{vrtx} (cm)	−13.89			Z_{vrtx} (cm)	16.38		
Run 65 581 event 322 592				Run 67 824 event 281 883			
muon $(-)$	21.4	0.57	6.00	electron $(+)$	52.3	−0.16	3.64
Jet 1 (SECVTX)	146.3	−0.56	1.21	Jet 1 (SECVTX)	78.8	−0.49	0.90
Jet 2 (SECVTX,SLT)	65.8	0.51	3.38	Jet 2	66.3	0.69	5.83
Jet 3	29.7	1.50	4.68	Jet 3 (SECVTX,SLT)	55.8	0.68	2.09
$E\!\!\!/_T$	70.2		3.78	$E\!\!\!/_T$	57.6		4.30
SLT (μ^-)	31.3	0.58	3.34	SLT (μ^-)	7.2	0.88	1.97
Z_{vrtx} (cm)	5.54			Z_{vrtx} (cm)	−10.56		
Run 46 818 event 221 912							
muon $(-)$	48.2	1.02	2.36				
Jet 1 (SECVTX,SLT)	55.4	−0.02	2.96				
Jet 2	41.7	0.27	5.08				
Jet 3	35.3	0.82	5.68				
$E\!\!\!/_T$	22.3		0.30				
SLT (μ^+)	10.5	0.06	2.93				
Z_{vrtx} (cm)	−17.28						

Table XIV shows agreement also between the number of jets with heavy flavor tagged by the SLT algorithm in the data and simulation (the SLT algorithm was not used to calibrate the simulation). However the numbers of SLT tags in the data have large errors because the ratio of tags due to heavy flavor to mistags is about 1/5. For jets with a supertag (SECVTX+SLT or JPB+SLT) the ratio of tags due to heavy flavor to mistags is about 2/1, and this allows a good cali-

TABLE XVIII. Characteristics of the $W+2$ jet events with a superjet rescued by removing the L2 trigger requirement.

	p_T (GeV/c)	η	ϕ (rad)
Run 61 525 event 116 807			
muon $(+)$	50.5	0.48	0.58
Jet 1 (SECVTX,SLT)	66.3	0.10	4.45
Jet 2	36.8	−0.71	1.87
$E\!\!\!/_T$	22.2		4.30
SLT (μ^-)	11.2	0.11	4.36
Z_{vrtx} (cm)	5.72		
Run 68 592 event 250 386			
muon $(-)$	57.5	−0.07	4.69
Jet 1	60.6	−1.08	4.09
Jet 2 (SECVTX,SLT)	42.5	−0.17	1.44
Jet 3	32.5	1.58	0.97
$E\!\!\!/_T$	36.1		1.12
SLT (μ^+)	7.9	−0.21	1.42
Z_{vrtx} (cm)	14.48		

TABLE XIX. Characteristics of the $W+2,3$ jet events with a superjet found in the plug electron sample.

	p_T (GeV/c)	η	ϕ (rad)
Run 69 941 event 66 919			
electron $(-)$	43.4	−1.33	0.77
Jet 1 (SECVTX,SLT)	84.5	−0.12	4.09
Jet 2	50.7	1.99	1.29
$E\!\!\!/_T$	11.6		4.53
SLT (μ^+)	13.5	−0.09	4.06
Z_{vrtx} (cm)	16.00		
Run 58 202 event 109 847			
electron $(+)$	65.9	1.45	1.43
Jet 1	32.6	0.28	4.84
Jet 2 (SECVTX,SLT)	30.8	−0.75	4.38
$E\!\!\!/_T$	12.5		4.73
SLT (e^-)	3.5	−0.63	4.49
Z_{vrtx} (cm)	−18.08		

bration of the efficiency for finding supertags in the simulation. We compare ratios of supertags to SECVTX (JPB) tags in the data and the simulation in order to cancel the contribution of the uncertainty of the simulated SECVTX (JPB) algorithms. Efficiencies for finding SLT tags in jets already tagged by SECVTX or JPB are listed in Table XV. We find that the efficiency for finding supertags in the data is (85 ± 5)% of the simulated efficiency. The small differences in the tagging efficiency between data and simulation in Table XV do not seem to be caused by a particular flavor type, because the relative fractions of b and c quarks are quite different in jets tagged by SECVTX and jet probability. The uniformity of the data-to-simulation scale factor for finding supertags across the three independent generic-jet samples also excludes any large dependence on the jet transverse energy. If we combine these three samples, we find that the efficiency for finding supertags in the data is (84 ± 5)% of the simulated efficiency for SECVTX tags and (86 ± 7)% for JPB tags. Since the heavy flavor composition of generic-jet data with a SECVTX tag (73% b quarks and 27% c quarks) is very similar to the composition of $W + \geq 2,3$ jet events with a SECVTX tag, the excess of $W + 2,3$ jet events with a supertag cannot be explained by correlations between the SLT and SECVTX algorithms unaccounted for by the simulation.

APPENDIX B: CHARACTERISTICS OF THE EVENTS WITH A SUPERJET

Tables XVI and XVII list the characteristics of the 13 events with a superjet. Four of these events are included in the data set used to measure the top quark mass [18].

Event 41 540/127 085 in Table XVI is classified in Ref. [18] as a dilepton event. In the present analysis, which uses tighter lepton selection criteria, the muon candidate appears to be due to punch-through of a stiff track inside the jet with $E_T = 144.5$ GeV. The fit of this event yields a top quark mass $M_{top} = 158.8$ GeV/c^2.

The other three events (65 581/322 592, 67 824/281 883, and 56 911/114 159 in Table XVII) contain an additional jet with $E_T \geq 8$ GeV and $|\eta| \leq 2.4$. The fit of these events in Ref. [18] yields $M_{top} = 152.7$, 170.1, and 156.7 GeV/c^2, respectively.

Table XVIII lists the characteristics of the two events found by removing the L2 trigger requirement for primary muons. The characteristics of the two additional events with a superjet and a primary plug electron are listed in Table XIX.

[1] S. L. Glashow, Nucl. Phys. **22**, 579 (1961); S. Weinberg, Phys. Rev. Lett. **19**, 1264 (1967); A. Salam, in *Elementary Particle Theory: Relativistic Groups and Analyticity (Nobel Symposium No. 8)*, edited by N. Svartholm (Almqvist and Wiksell, Sweden, 1968), p. 367; M. Gell-Mann, in *QCD, 20 Years Later*, edited by P. M. Zervas and H. A. Kastrup (World Scientific, Singapore, 1993).

[2] CDF Collaboration, F. Abe *et al.*, Phys. Rev. Lett. **70**, 4042 (1993); **73**, 2296 (1994); **76**, 3070 (1996); **81**, 1367 (1998).

[3] F. Abe *et al.*, Phys. Rev. D **50**, 5550 (1994); D. Cronin-Hennessy *et al.*, Nucl. Instrum. Methods Phys. Res. A **443**, 37 (2000). The luminosity is derived using the total $p\bar{p}$ cross section value 80.03 ± 2.24 mb.

[4] F. Abe *et al.*, Phys. Rev. D **50**, 2966 (1994); Phys. Rev. Lett. **73**, 225 (1994).

[5] F. Abe *et al.*, Phys. Rev. Lett. **74**, 2626 (1995).

[6] F. Abe *et al.*, Phys. Rev. Lett. **80**, 2773 (1998).

[7] T. Affolder *et al.*, Phys. Rev. D **64**, 032002 (2001).

[8] F. Bonciani *et al.*, Nucl. Phys. **B529**, 450 (1998); E. Berger and H. Contopanagos, Phys. Rev. D **54**, 3085 (1996); S. Catani *et al.*, Phys. Lett. B **378**, 329 (1996); E. Laenen *et al.*, *ibid.* **B321**, 254 (1994).

[9] S. Abachi *et al.*, Phys. Rev. Lett. **79**, 1203 (1997).

[10] J. Gunion *et al.*, *The Higgs Hunter's Guide* (Addison-Wesley, Reading, MA, 1990).

[11] E. Eichten and K. Lane, Phys. Lett. B **388**, 803 (1996).

[12] Particle Data Group, D. E. Groom *et al.*, Eur. Phys. J. C **15**, 1 (2000).

[13] D. Amidei *et al.*, Nucl. Instrum. Methods Phys. Res. A **271**, 387 (1988); Fermilab Report 94/024-E (1994).

[14] D. Amidei *et al.*, Nucl. Instrum. Methods Phys. Res. A **350**, 73

(1994); P. Azzi *et al.*, *ibid.* **A360**, 137 (1994).

[15] F. Abe *et al.*, Phys. Rev. D **45**, 1448 (1992).

[16] F. Abe *et al.*, Phys. Rev. Lett. **70**, 1376 (1993).

[17] F. Abe *et al.*, Phys. Rev. Lett. **80**, 2767 (1998).

[18] T. Affolder *et al.*, Phys. Rev. D **63**, 032003 (2001).

[19] T. Sjöstrand, Comput. Phys. Commun. **39**, 347 (1986); T. Sjöstrand and M. Bengtsson, *ibid.* **43**, 367 (1987); **46**, 43 (1987).

[20] G. Marchesini and B. R. Webber, Nucl. Phys. **B310**, 461 (1988); G. Marchesini *et al.*, Comput. Phys. Commun. **67**, 465 (1992).

[21] F. A. Berends, W. T. Giele, H. Kuijf, and B. Tausk, Nucl. Phys. **B357**, 32 (1991).

[22] J. Benlloch, *Proceedings of the 1992 DPF Meeting, Batavia, IL, 1992*, edited by C. H. Albright *et al.* (World Scientific, Singapore, 1993), p. 1091.

[23] A. D. Martin, R. G. Roberts, and W. J. Stirling, Phys. Lett. B **306**, 145 (1993); **309**, 492(E) (1993).

[24] A. Ballestrero *et al.*, hep-ph/0006259; M. Mangano, hep-ph/9911256.

[25] M. Seymour, Nucl. Phys. **B436**, 163 (1995); M. Mangano and P. Nason, Phys. Lett. B **285**, 160 (1992).

[26] P. Avery, K. Read, and G. Trahern, Cornell Internal Note CSN-212, 1985. We use Version 9_1 of the CLEO simulation and our own lifetime database.

[27] J. Ohnemus and J. F. Owens, Phys. Rev. D **44**, 1403 (1991); **44**, 3477 (1991); **43**, 3626 (1991); B. Mele *et al.*, Nucl. Phys. **B357**, 409 (1991); S. Frixione *et al.*, *ibid.* **B383**, 3 (1992); **B410**, 280 (1993).

[28] T. Stelzer, Z. Sullivan, and S. Willenbrock, Phys. Rev. D **56**, 5919 (1997); M. Smith and S. Willenbrock, *ibid.* **54**, 6696 (1996).

[29] M. Mangano, Nucl. Phys. **B405**, 536 (1993).

[30] The probability is estimated with Monte Carlo pseudoexperi-

ments which include both Poisson fluctuations and Gaussian uncertainties in the prediction. Using these experiments we derive the probability of observing a likelihood $\mathcal{L} = \Pi_{i=1}^{4}[\mu_{i}^{n_{i}} \exp^{-\mu_{i}}/n_{i}!]$, where n_i and μ_i are the observed and predicted numbers of tags in the ith jet bin, no larger than that of the data.

[31] N. H. Kuiper, Proc. Kon. Ned. Akad. Wetensch., Ser. A: Math Sci. **63**, 38 (1962).

[32] W. T. Eadie, D. Dryard, F. E. James, M. Roos, and B. Sadoulet, *Statistical Methods in Experimental Physics* (American Elsevier, New York, 1971).

[33] W. H. Press, S. A. Teutolsky, W. T. Vetterling, and B. P. Flannery, *Numerical Recipes* (Cambridge University Press, Cambridge, England, 1992).

[34] The central fast tracker (CFT) is a hardware processor which uses fast timing information from the CTC as input and provides a list of $r - \phi$ tracks to the second level trigger (L2). The L2 muon trigger required CFT tracks with $p_T \geq 9.2 \, \text{GeV}/c$ in the first part of the collider run and $p_T \geq 12 \, \text{GeV}/c$ in the remaining 80% of the data taking period.

[35] A. D. Martin, R. G. Roberts, and W. J. Stirling, Phys. Lett. B **354**, 155 (1995).